Measurement of Kr-83m Doping in Xenon Gas for Calibration and Tracer Applications

Sergej Schneider

Bachelor thesis

Institut für Kernphysik
Mathematisch-Naturwissenschaftliche Fakultät
Westfälische Wilhelms-Universität Münster

3. August 2012

Westfälische
Wilhelms-Universität
Münster

Referent: Prof. Dr. C. Weinheimer

Korreferent: Prof. Dr. J. Wessels

Contents

1 Introduction

Since the 1930s, when the concept of dark matter was introduced by Fritz Zwicky to explain the average velocity of galaxies in the Coma Cluster, the scientific world has wondered about its nature and composition. Since then more and more evidence has been found suggesting the existence of non-baryonic dark matter and a variety of theories have been developed in an attempt to characterize it. One very promising theory, which comes naturally from theoretical extensions of the Standard Model of particle physics, proposes that the so called Weakly Interacting Massive Particle (WIMP) should be responsible for this huge amount of unknown mass in the universe. Up to this day no definitive experimental detection of the WIMP has been found, which makes it an interesting field of research.

One of the many experiments that follows this path is the XENON Dark Matter Project, an international collaboration with its detector installed at Laboratori Nazionali del Gran Sasso (LNGS) in Italy. It tries to detect dark matter directly by measuring the energy of a nuclear recoil deposited when a WIMP scatters off of the xenon target in a time projection chamber (TPC). For calibrating the TPC at XENON100 regarding its light yield response, radioactive sources can be brought near the detector. With an increasing volume, low energy calibration in the inner volume of the detector becomes difficult. Due to the self shielding effect of xenon, a low energy radioactive source will not penetrate the detector. Therefore, ^{83m}Kr can be introduced into the TPC to allow an internal low energy calibration.

Due to its small cross section a WIMP scattering event is expectably rare, which leads to a requirement of extremely small background in the detector. Since xenon always contains traces of radioactive ^{85}Kr, a very high xenon purity is essential in order to achieve the small background rate which is required for the next step of the XENON Dark Matter Project: XENON1T, a detector in ton-scale which will increase the sensitivity by two orders of magnitude. The XENON group in Münster is addressing this problem by building a krypton distillation column and a gas system including a purification unit, which will achieve the purity requirements for XENON1T.

The aim of this bachelor thesis was the construction and testing of a ^{83m}Kr pipette that can be attached to the XENON100 detector in Gran Sasso for a uniform internal gamma calibration of the TPC at relatively low energies (tens of keV) and for tracer applications to characterize the krypton distillation column, a necessary ingredient for XENON1T. For testing the pipette a scintillation detector was used with gaseous xenon as scintillation material and a photomultiplier tube which is sensitive to its scintillation light.

2 Theoretical Background

2.1 Dark Matter

A great deal of evidence for non baryonic dark matter has been found since the first proposal of Fritz Zwicky in 1933. Some of the very important cases will be discussed in this section in order to get an understanding of the motivation for the search for dark matter.

2.1.1 Evidence

Historically, the first hint for the existence of dark matter was the velocity of the stars in the milky way, observed by Jan Oort in 1932[Oort1932] and was later extended as standard behaviour of spiral galaxies by Vera Rubin in the 1970s. With a given mass distribution $M(r)$ one would expect a velocity $v(r)$ given by Newtonian mechanics as

$$v(r) = \sqrt{GM(r)/r}. \tag{2.1}$$

Since the majority of the luminous mass is accumulated in the galactic centre and decreases for large distances, a decreasing velocity is expected. Contrary to the expectation, measurements showed a flat behaviour of the rotation curves for large radii. This leads to the conclusion that there should be a halo of dark matter in galaxies that accounts for the missing mass. The flatness of galactic rotation curves has a big importance concerning the detection of dark matter on earth, as only this observation implies the assumption that dark matter could be found on earth due to its position in the galaxy. As an example for a typical spiral galaxy, figure 1 shows the rotation curve of the galaxy NGC6503.

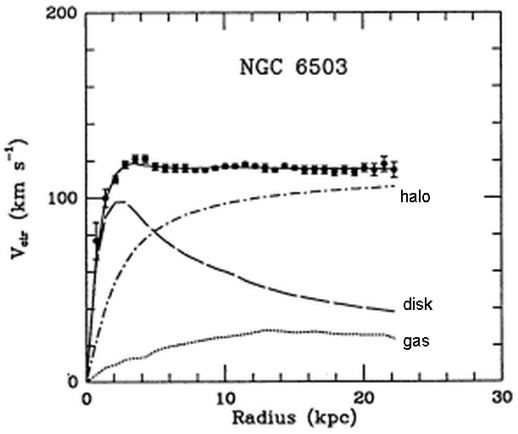

Figure 1: Rotational curve of the spiral galaxy NGC6503 fitted with a three parameter dark-halo fit.[Beg1991]

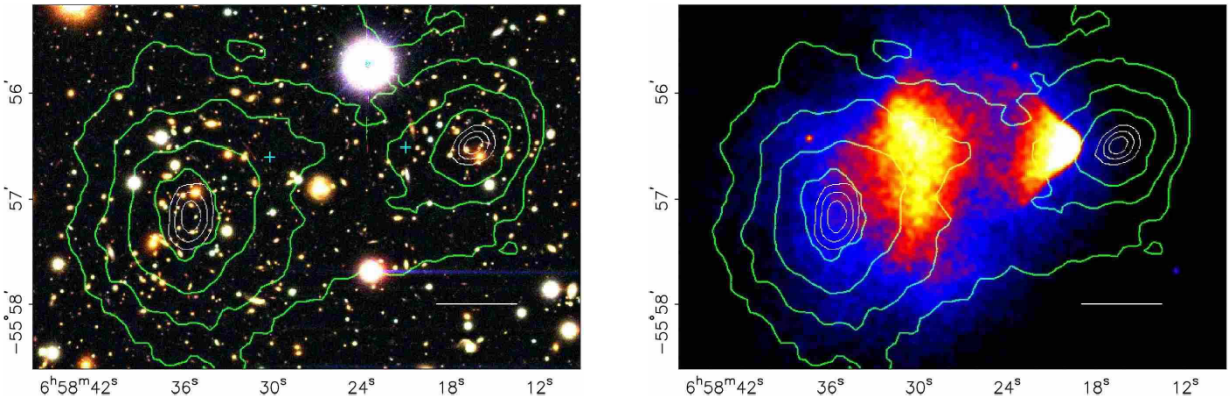

Figure 2: Color image and X-Ray image of Bullet Cluster 1E0657-558. The green contours show the weak lensing reconstruction. The centre of mass is surrounded by the white contours, indicating the peak of the weak lensing effect. The biggest density of X-Ray emitting gas is represented by the yellow/white area.[Clo2006].

Another very convincing evidence for the existence of and especially the amount of dark matter in an even bigger scale is the characteristic of galactic clusters, where up to thousands of galaxies are gravitationally bound to a group. Zwicky found by analyzing the Coma Cluster for the average velocity of its galaxies, that to fulfill the virial theorem

$$2\,\langle E_K\rangle = -\,\langle U\rangle \tag{2.2}$$

with the kinetic energy E_K and the potential energy U over 400 times more mass is needed than the luminous mass can account for[Zwi1933] (with the current value of the Hubble-constant H_0 it would be over 50) and proposed with that the idea of dark matter.

While Zwicky just suggested dark matter to be only non-luminous, later observations demanded further characteristics. Particularly the Bullet Cluster (as seen in figure 2) as a result of a collision of two separate galaxy clusters shows a behaviour that could not be explained satisfyingly without the presence of dark matter.

Based on the theory of general relativity, light is affected in its propagation by large accumulations of mass. This gravitational lensing effect can therefore be used to detect large interstellar objects. If a massive object lies is in between a luminous object and an observer, it can bend the light in a way that the observer sees the luminous object as a ring around the massive object (strong lensing). In larger objects like galaxy clusters the mass distribution is more complex. Here, only small statistical distortions are observed (weak lensing). In this case a large number of luminous objects has to be analyzed to draw conclusions about the mass distribution.

By comparing the mass distribution of the Bullet Cluster from gravitational lensing to its distribution of visible mass, a clear separation of both was observed. While in the centre of the collision X-Ray emitting gas, which is the dominant component of luminous mass of both clusters, is accumulated and slowed down because of its electromagnetic interaction, the centre of mass of both clusters, as measured by gravitational lensing, passed through each other without a nominal effect.

The most precise prediction of the amount of dark matter in the universe and one of the strongest arguments for the existence of dark matter is given by measurements of the cosmic microwave background (CMB). The CMB is a radiation background originating from the recombination phase of the early Universe, where matter was nearly isotropically distributed as plasma. As the universe cooled down and the plasma recombined into atoms, it became transparent to photons and the CMB was released. The CMB is the best measured black body radiation of all time at a temperature of $T = 2.725\,\mathrm{K}$ (measurement from WMAP shown in figure 3). Still tiny fluctuations in the region of μK can be observed. These fluctuations are responsible for all structure formation in the later development of the universe. By analyzing the angular moment of the power spectrum of the anisotropies, statements about the energy composition of the universe can be made. From it the conclusion can be drawn that the overall mass-energy content is composed by only 4.6 % regular baryonic matter while 23% has to be the yet unknown dark matter.

Furthermore, from measurements of redshift of type IA supernovae another statement is motivated. The expansion of the universe indicates its flatness. Therefore, the remaining 73 % of the mass-energy content has to be made out of an unknown form of energy, called dark energy.

The results from WMAP are in impressive agreement with the ΛCDM (Lambda Cold Dark Matter) model. It is the slimpest cosmological model which explains large structure building in the universe and its accelerating expansion.

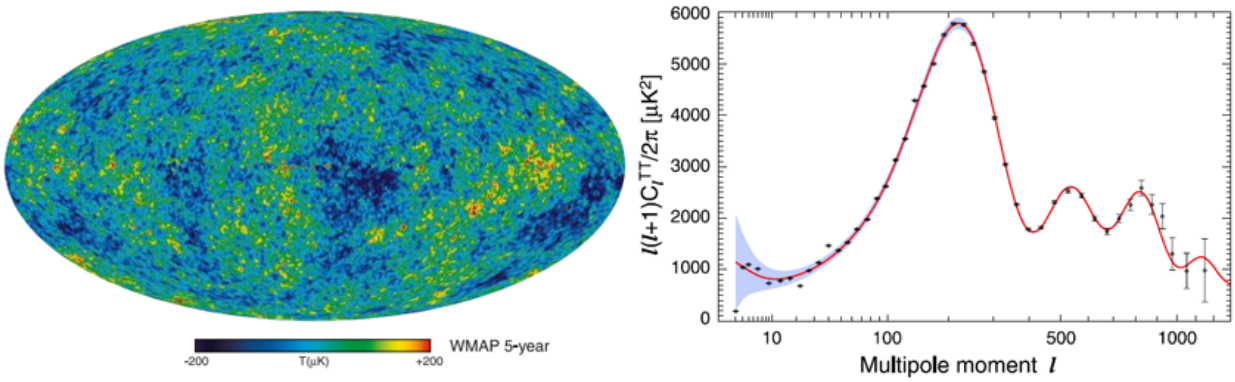

Figure 3: *Left:* WMAP 5-year map of the Cosmic Microwave Background. The fluctuations in temperature lie in between $\pm 200\,\mu K$ [Hin2008]; *Right:* The 7-year angular power spectrum from WMAP. The solid red line is the best fit given by the ΛCDM model [Lar2010].

2.1.2 The WIMP as a Candidate for Dark Matter

While a minor part of the missing-mass-problem can be explained by already known particles such as neutrinos or conventional baryonic matter in non-luminous stellar objects (black holes, brown dwarfs, neutron stars etc.), the major part simply cannot. This indicates the necessity of physics beyond the standard model. The standard model (SM), although being the foundation of modern particle physics, needs to be extended as its limitations of describing a complete picture of the universe have become more evident in recent years. The supersymmetry (SUSY) as extension to the SM appeals to most physicists because of its elegance and potential to solve various problems in particle physics. In particular it gives naturally some potential candidates for the searched dark matter. SUSY postulates the existence of superpartners to every boson or fermion of the SM whose spin differs by half a unit, making a fermion the superpartner of a boson and vice versa. In a perfect symmetry the superpartner and the SM particle would have identical masses. Due to the fact that no SUSY-particle has yet been found in any accelerator, their mass has to be significantly higher in the region of $\mathrm{TeV/c^2}$, which would make it a broken symmetry.

Of all theoretical particles postulated by SUSY the lightest supersymmetric particle (LSP) such as the neutralino is a natural candidate for dark matter due to its stability in cosmological scales. Furthermore it has no electric charge and is only sensitive to weak interaction besides gravitational effects. All properties that are necessary for explaining the observed behaviour described in chapter 2.1.1. These properties make the LSP a Weakly Interacting Massive Particle (WIMP).

2.1.3 Detection of Dark Matter

Due to the importance of dark matter for understanding the mass-energy content in our universe many attempts have been made to experimentally detect it. Those experiments follow two basic strategies.

Indirect detection experiments look for signatures of the annihilation or decay products of dark matter, preferably in the centre of massive objects. There, the accumulation of dark matter is expected to be higher and thereby increasing the probability of an annihilation or decay.

Direct detection experiments on the other hand are looking for effects of the interaction between dark matter and a terrestrial target.

According to theory, the earth should be penetrated by WIMPs due to its position in our galaxy, where interaction with baryonic matter, although with a tiny probability, can happen because of weak interaction. The detection rate R for WIMP-nucleus scattering is dependent on the average velocity of the WIMPs relative to the detector medium $\langle v \rangle$ and the local WIMP energy density ρ_0

$$R \propto \frac{\rho_0 \sigma \langle v \rangle}{m_\chi m_N}, \tag{2.3}$$

where σ is the cross section and m_χ / m_N the mass of the WIMP/nucleus. It is quite difficult to predict it in advance, because both energy density and velocity of dark matter in our narrow space in the milky way cannot be stated with absolute certainty. But because of the very small cross section, WIMP-nucleus scattering events are expected to be very rare.

To compensate for this small cross section direct detection experiments have to have a very high sensitivity for a WIMP-nucleus scattering. For this, the detector should show a very low radioactive background and at the same time should be operated at a low threshold for nuclear recoils. To obtain a relatively high cross section the target medium should have a preferably high mass number. To distinguish nuclear recoils from electronic recoils, a combination of two excitation channels (scintillation, ionization or heat) has to be used.

One class of detectors that fulfill these requirements are liquid noble gas detectors.

2.2 XENON Dark Matter Project

2.2.1 XENON100

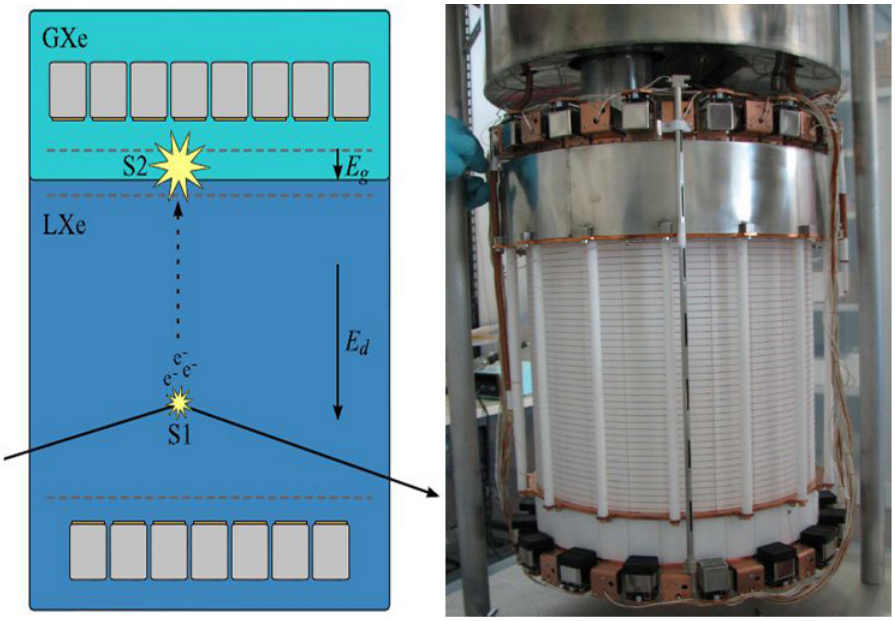

Figure 4: *Left:* Measurement principle of a dual-phase xenon ionization scintillation detector; *Right:* Picture of the XENON100 inner detector structure.[Pla2012]

The XENON Dark Matter Project is a direct detection experiment, currently running the XENON100 detector which is installed in an underground laboratory in Gran Sasso, Italy. The goal is to detect WIMPs by looking for the ionization and scintillation caused by a WIMP interacting with a xenon nucleus.

Xenon has some valuable properties as detector medium. It is the heaviest noble gas with solely stable isotopes appearing in nature, so that in liquid form it has a high density of $3 \dot{g}/cm^3$, which is beneficial for nuclear cross section, without producing background through radioactive decay. The detector is build as a dual phase time projection chamber (TPC) with liquid and gaseous xenon and is monitored by multiple photomultiplier tubes (PMT) (see figure 4). The inner surface is covered with PTFE (polytetrafluoroethylene, commonly known as Teflon) to improve the light collection due to its high reflectivity for xenon scintillation light.

If a nuclear interaction happens in the liquid phase of the TPC, a xenon atom gets excited, causing a direct scintillation signal (S1) which will mostly be detected by the bottom PMTs because of high internal reflection at the liquid surface ($n_{UV} = 1.67$). With an assumed relative WIMP velocity of about 340 km/s, a scattering event should deposit E $<$ 50 keV of energy in the detector. Furthermore, the interaction generates ionisation electrons. While the electric field

in the region of liquid xenon is just as high to cause a drift of the electrons to the surface, it increases drastically just below the surface. This extraction field provides enough energy for the electrons to cause a second scintillation (S2) in the gaseous phase.

The S2 signal of a nuclear scattering event is significantly smaller than of an electron scattering, because it leads to a higher ionization density in the liquid xenon, where more ionized electrons can directly recombine. Consequently, the different ratio of S1/S2 signals allow a discrimination of electric and nuclear scattering events. The time delay between S1 and S2 in combination with the arrays of PMTs allows a three dimensional reconstruction of an event.

With XENON10 the basic detector principle was successfully tested and with an amount of 5.4 kg of liquid xenon in the sensitive volume a sensitivity of $\sigma = 4.5 \cdot 10^{-44}\,\mathrm{cm}^2$ for WIMPs with a mass of $30\,\mathrm{GeV/c}^2$ was achieved[Apr2007]. To significantly reduce the radioactive background the detector volume had to be increased.

For that purpose the XENON100 detector was designed with 62 kg of liquid xenon in the sensitive volume monitored by 178 PMTs. The background is strongly reduced by the shielding effect of 1.4 km of rock from Gran Sasso itself, the choice of very low radioactive materials and the self-shielding effect of liquid xenon. Therefore, in XENON100 only 62 kg of the total 161 kg xenon is used as target volume, while the rest serves as active veto and innermost shield monitored by additional 64 PMTs. In 2012 the XENON Dark Matter Project set the most stringent limits regarding the possible spin-independent WIMP-nucleon cross section for $55\,\mathrm{GeV/c}^2$-WIMPs to $\sigma = 2.0 \cdot 10^{-45}\,\mathrm{cm}^2$ after 225 live days of data (see figure 5) while no dark matter signal was observed and by that questioned again the claimed discoveries of DAMA/Libra and CoGeNT.

In the near future the detector will be replaced by the XENON1T detector with an amount of 1 T xenon in the fiducial volume to reach an even higher sensitivity of $\sigma = 2 \cdot 10^{-47}\,\mathrm{cm}^2$[Ari2012]. This will lead to a high discovery potential of the XENON1T detector. With this progress the xenon purity begins to set the limit for the reachable sensitivity.

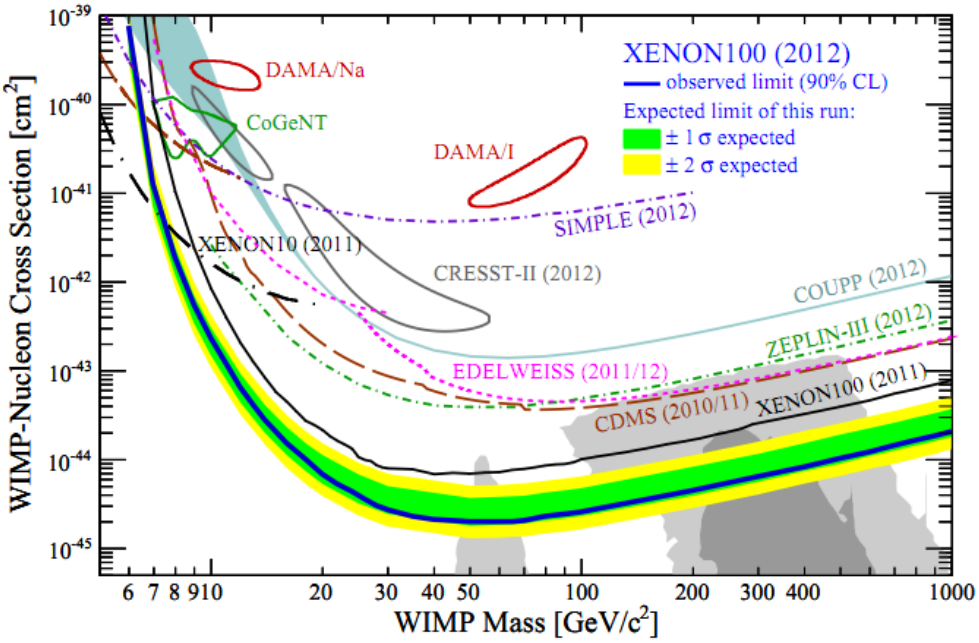

Figure 5: Achieved sensitivity for spin-independent WIMP-nucleon cross section from various experiments and theoretical predictions (grey areas)[Apr2012a]).

2.2.2 Calibration Methods

To calibrate the XENON100 detector several sources are used in order to get information about its response to nuclear recoils, electron recoils and the light yield as well as the purity of the xenon. In XENON100 a copper pipe surrounds the chamber through which a solid radioactive source can be placed near the detector at several azimuthal positions.

The nuclear recoil band can be calibrated with a ^{241}AmBe source. ^{241}Am decays via emission of alpha particles. ^{9}Be has a large cross section for the absorption of alpha particles. The nuclear reaction that leads to the emission of a neutron is

$$^{9}Be +^{4} He \rightarrow^{12} C + n + \gamma. \tag{2.4}$$

At certain locations lead blocks are attached to absorb unwanted gamma rays.

The electron recoil band on the other hand is calibrated with a ^{60}Co source. It decays via emission of an electron and furtheron two γ rays (1.17 MeV and 1.33 MeV). Those relatively high energies allow an only just sufficient penetration of the XENON100 detector.

To infer the electron lifetime inside the TPC and therefore the purity of the liquid xenon a ^{137}Cs is commonly used. The gamma photons emitted by the decay of ^{137m}Ba (^{137}Cs $\rightarrow^{137m}$ Ba $\rightarrow^{137}$ Ba) with an energy of 661.7 keV cause events in the TPC. By analysing the S2 response to the known gamma lines, conclusions can be drawn about the drift length.

To calibrate the light yield response at different energies various calibration sources like ^{60}Co, ^{137}Cs or ^{232}Th are commonly used. All mentioned calibration sources only allow light yield calibration with energies much higher than the expected energy deposit by WIMP scattering. With increasing size of the detector, calibration at low energies becomes a bigger issue. Due to the self shielding effect of xenon, liquid xenon would have to be doped with a low energy radioactive source and introduced to the active medium to ensure a calibration in that particular volume. Therefore ^{83m}Kr suits perfectly due to its practicel half-life and low energy electron emission (see chapter 2.3).

2.2.3 Distillation Purification of Xenon for Krypton

Since xenon is a trace gas which is obtained through the process of fractional distillation of air, even already purified, commercially available xenon has an abundance of natural krypton in the region of a few parts per billion (ppb) with a ratio of ^{85}Kr/Kr of about 10^{-11}. The amount of the radioactive ^{85}Kr is mainly produced artificially in nuclear fission.
It disintegrates through beta decay with an endpoint energy of 687.4 keV and has a half life of 10.76 years. It can therefore generate a background signal in the fiducial volume that cannot be distinguished from a potential WIMP-nuclear scattering event. This is why krypton has to be removed below the ppt level to achieve a xenon purity that allows the intended sensitivity of XENON1T.
In XENON100 the purification is done by a cryogenic distillation column from Taiyo Nippon Sanso®[Abe2009], taking advantage of the different boiling points of krypton and xenon. At 1 atm the boiling point of krypton is at $T_{\mathrm{Kr}} = 120\,\mathrm{K}$ while the one of xenon is at $T_{\mathrm{Xe}} = 165\,\mathrm{K}$. Therefore a tower is used with a reboiler at the bottom and a condenser at the top maintaining a constant temperature profile. Xenon is supplied to the feed point at half height after being pre-cooled down to nearly its boiling point. Inside the column a vapor-liquid equilibrium is maintained. The temperature gradient leads to a separation of xenon with a higher concentration of krypton at the top and xenon with a lower concentration of krypton at the bottom. The purified xenon can then be extracted and supplied to the gas system while the off-gas with a higher concentration is separately stored. A schematic of the distillation column is shown in figure 6.

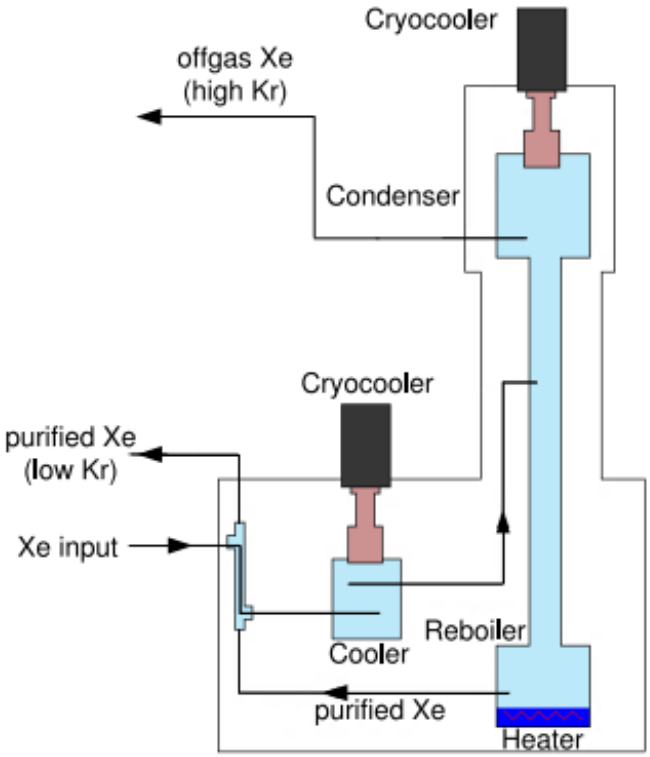

Figure 6: Schematic layout of the cryogenic distillation column used to separate krypton from xenon.[Apr2012b]

In XENON100 the distillation column is 2 m tall with a diameter of 2 cm and throughput of 0.6 kg/h. To process 170 kg of xenon used in XENON100 the distillation column takes under 2 weeks.

Since XENON1T requires both a higher xenon purity and a faster distillation due to the much bigger detector volume, a new distillation column must be designed which meets the strict requirements. For that the dimensions of the column will be changed while using the same principle. To reach the intended purity, the column will have to be 3 m tall with a diameter of 4 cm to allow a purification flow rate of about 3 kg/h and a krypton reduction factor of 10^4. Under those conditions the whole amount of xenon in XENON1T can be purified in about 5 weeks.

2.2.4 ^{83m}Kr Tracer Method for Characterization of the Kr Column

The krypton distillation column at XENON100 was designed to reduce the amount of krypton down to the parts per trillion (ppt) level. Measuring the separation factor of the column based on the difference in concentration of ^{85}Kr with a half-life of several years and concentrations that low is quite challenging. Introducing additional ^{85}Kr is not an option, because it would contaminate the used xenon. As the distillation column works independently for all krypton isotopes, ^{83m}Kr can be used as a tracer to evaluate the separation efficiency. Its benefit is obviously that with a half-life of just 1.83 hours there is no risk of long term contamination. Therefore, gaseous xenon gets doped with a certain amount of ^{83m}Kr before supplying to the distillation column. Then the activity of the doped xenon is measured before and after the distillation. The ratio between the activity of ^{83m}Kr before the purification to the activity after it then gives the separation factor for krypton in general.

2.3 Radioactive Decay of ^{83}Rb and ^{83m}Kr

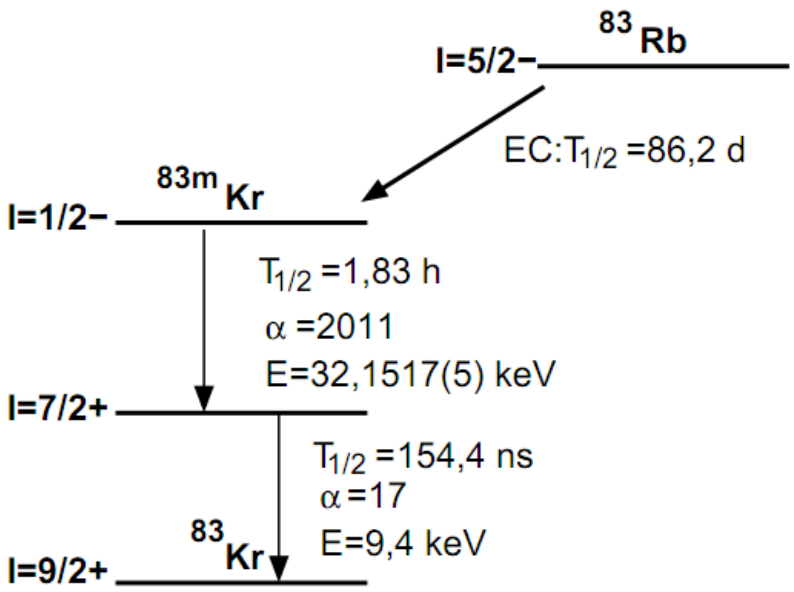

Figure 7: Decay scheme of ^{83}Rb to the stable ^{83}Kr. With a probability of 74.8 % the decay goes over the radioactive ^{83m}Kr.[Ost2008]

The excited ^{83m}Kr used for calibration is obtained from a radioactive ^{83}Rb source. Since a radioactive decay is a statistical process, it can only be stated with a certain probability which is proportional to the decay constant λ:

$$\mathrm{P} \propto e^{-\lambda t}. \tag{2.5}$$

The decay constant λ is connected to the half-life $t_{1/2}$:

$$\lambda = \ln(2)/t_{1/2}. \tag{2.6}$$

A very important property of a radioactive source is its activity A which is defined as decays per second, given by

$$A(t) = N(t) \cdot \lambda = N_0 \cdot e^{-\lambda t} \cdot \lambda. \tag{2.7}$$

^{83}Rb disintegrates with a half-life of $t_{1/2}(\mathrm{Rb}) = 86.2\,\mathrm{d}$ solely through electron capture (EC), where an inner shell electron is captured by a proton. This leads to the conversion of the proton to a neutron while emitting an electron neutrino ν_e.

$$^{83}_{37}\mathrm{Rb} + e^- \rightarrow {}^{83}_{36}\mathrm{Kr} + \nu_e \tag{2.8}$$

With a branching ration of 74.8 % the decay of ^{83}Rb leaves the resulting krypton atom in the short lived isomeric state ^{83m}Kr at 41.55 keV. ^{83m}Kr disintegrates in two steps mainly via emission of conversion electrons with the energy of $E_1 = 32.15\,\mathrm{keV}$ after a half-life of $t_{1/2}(32.15\mathrm{keV}) = 1.83\,\mathrm{h}$ and subsequently with an energy of $E_2 = 9.4\,\mathrm{keV}$ after a half-life of $t_{1/2}(9.4\mathrm{keV}) = 154.4\,\mathrm{ns}$. Conversion electrons are produced by the process of internal conversion (IC), where an inner shell electron interacts with an excited nucleus. It can transfer its energy without emission of gamma rays, giving the conversion electron a well specified discrete kinetic energy

$$E_{kin} = E_N - E_B \tag{2.9}$$

where E_γ is the energy of the nucleus and E_B is the binding energy of the electron. The excitation via IC competes with that of gamma decay. It is quantified with the internal conversion coefficient α which is defined as the ratio of the number of excitations via emission of electrons to excitations via emission of photons. The IC can furthermore lead to the emission of Auger electrons, when the vacancy of the missing conversion electron is filled with a higher shell electron. ^{83m}Kr has an internal conversion coefficient for its first decay of 2011, meaning it deexcites almost exclusively by IC. Its second decay with $\alpha = 17$ is still dominated by IC but in rare cases the energy is carried by gamma rays.

3 Experimental Setup

The setup described below was designed and built under supervision of Ph.D. student Stephan Rosendahl, who is going to use it for analyses in context of his Ph.D. thesis.

3.1 A ^{83m}Kr Pipette for Calibration of XENON100

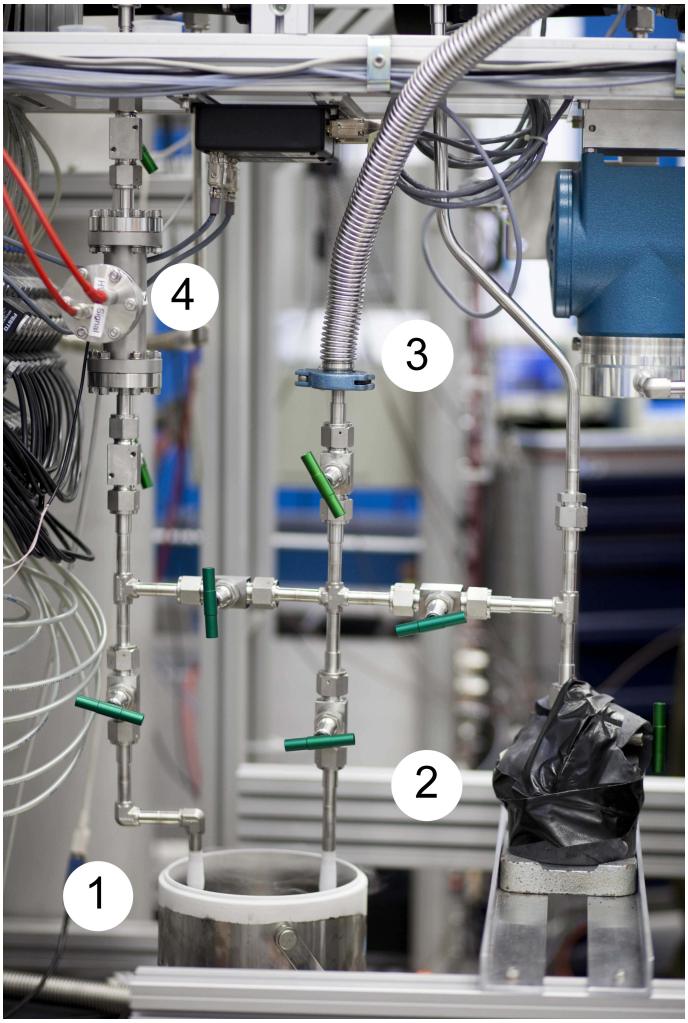

Figure 8: Krypton-collecting system with cold trap (1), ^{83}Rb source (2), vacuum pump (3) and krypton detector (4).

The main purpose of building the pipette was to allow the collection of ^{83m}Kr outside of LNGS and then bring the calibration source in the underground laboratory. Due to safety regulations, the radioactive ^{83}Rb source could not be used in the underground lab. The collection was supposed to be enhanced by operating it with a cold trap using liquid nitrogen. This set some general requirements regarding the geometry and features the pipette needed to have. The result of the pipette, connected to the gas system in Münster is seen in figure 8.

Before collecting krypton, evacuation of the system was necessary, especially in the case of using the pipette for XENON100 because parts of the system would be exposed to air in the process of being delivered to LNGS. To prevent contamination of the xenon gas, these parts would have to be evacuated before being opened to the gas circuit. For testing the pipette in Münster the evacuation allowed the assumption of evenly distributed ^{83m}Kr in the pipes in a reasonable time and with that a practical analysis of the benefit of the cold trap and the efficiency of the ^{83m}Kr detector. Therefore four open ends were implemented in the system. One was connected to the ^{83}Rb source, two for gas in- and output and the last was connected to a vacuum pump.

To assure that the pipette was leak-tight all parts were orbitally welded and connected with VCR-fittings from Swagelok®. The stainless steel pipes with an inner diameter of 10 mm were electropolished to improve the vacuum due to the beneficial surface and to prevent introducing impurities to the system. The finished pipette was cleaned with an ultrasonic cleaner and leak-checked with a helium leak detector from Oerlikon Leybold Vacuum®. With it, the leakage rate could be determined to be just 10^{-8} mbar $\cdot$ L/s. It also served as a vacuum pump producing a vacuum of p $\approx 5 \cdot 10^{-3}$mbar.

^{83m}Kr, as explained in chapter 2.3, is a decay product of ^{83}Rb. Because of the relatively long half-life of ^{83}Rb it had to be ensured that no rubidium would be collected in the pipette and with that contaminating the xenon for a long time. To prevent this from happening, the radioactive ^{83}Rb source was embedded in zeolite pellets with a pore size of 0.5 nm covered by a PTFE membrane with a pore size of 220 nm (as seen in figure 9). Zeolite is an aluminosilicate mineral with a crystal structure. It can trap ^{83}Rb as counter cation to the aluminosilicate anion. ^{83m}Kr on the other hand, can emanate the zeolite due to its porous structure.

Figure 9: *Left:* ^{83}Rb source embedded in zeolite pellets[Han2011]. *Right:* Top of the rubidium source with the protective PTFE membrane filter[Ave2012].

Studies have shown that the source does not release ^{83}Rb at a detectable level[Han2011] while ^{83m}Kr can emanate the source nearly completely[Ven2005]. However, non negligible variations from source to source have been observed in further tests. They suggested an emanation rate of the source used in Münster to be $\epsilon = (70 \pm 5)\%$.

When prepared on May, 6$^{\text{th}}$ 2011, the activity of the radioactive rubidium source was measured to be $A = (2870.71 \pm 0.26)\,\text{kBq}$. With the known half-life of $t_{1/2}(^{83}\text{Rb}) = 86.2\,\text{d}$, the current activity could be calculated for every measurement-day to get an accurate prediction of the amount of ^{83m}Kr that could be collected.

3.2 Functional Principle of the ^{83m}Kr Detector

For analyzing the decay of ^{83m}Kr, a scintillation detector (as seen in figure 10) was used where gaseous xenon served as scintillation material. A R8520-06-Al Hamamatsu® photomultiplier tube (PMT) sensitive to the scintillation light from xenon with $\lambda = 178\,\text{nm}$ then detected the light output. In the following, the components will be explained.

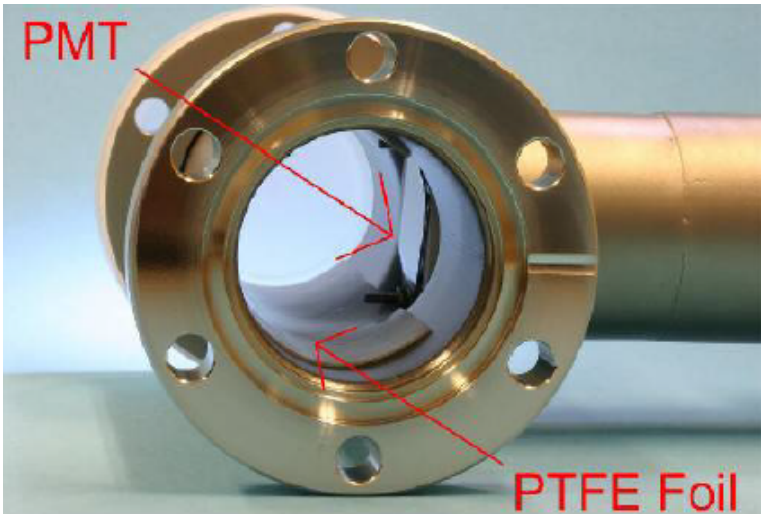

Figure 10: Opened ^{83m}Kr detector with visible PMT and high reflective PTFE.

3.2.1 Xenon as Scintillation Material

Xenon has some valuable properties that allow it to be operated as a scintillation detector. It is the heaviest noble gas with solely stable isotopes appearing in nature, so that in standard reference conditions gaseous xenon has a high density of $5{,}894\,\text{g/l}^3$ without producing background through radioactive decay. Like all noble gases, xenon gets excited by charged particles as atom but with gas pressure of about 1 bar deexcites as excimers which describes an excited molecular

state.

A charged particle, with an energy level relevant for our case ($<$ MeV), interacts with the xenon gas through interaction with its shell electrons or with the nuclei itself and in the case of electrons, looses its energy mainly through inelastic scattering. This process finally leads to excited xenon atoms forming excited dimers with relaxed xenon atoms in a 3-body collision.

$$Xe^* + Xe + Xe \rightarrow Xe_2^* + Xe \tag{3.1}$$

While subsequently decaying, the excimer emits scintillation photons with a wavelength of $\lambda_{GXe} = 178\,\text{nm}$ with a FWHM of 10 nm[Mon2007]:

$$Xe_2^* \rightarrow 2Xe + h\nu. \tag{3.2}$$

Due to this process, xenon is practically own scintillation light. Photons of this wavelength are also called vacuum ultraviolet (VUV) photons due to their very short attenuation length in air. The average energy W_{ph} which is required for an electron to generate a photon was determined to be 21.6 eV (in liquid xenon)[Apr2009]. In gaseous xenon with a pressure of 1 bar electrons with an energy of a few keV have an attenuation length of $\lambda < 1\,\text{cm}$. As the lifetime of excimers lies in the region of a few ns (3/27 ns for singlet/triplet state), xenon is one of the fastest scintillators. As well as direct excitation, primary ionization can also lead to an excited xenon atom that can form excimers as described in equation 3.1.

$$\begin{aligned} Xe^+ + Xe &\rightarrow Xe_2^+ \\ Xe_2^+ + e^- &\rightarrow Xe^{**} + Xe \\ Xe^{**} &\rightarrow Xe^* + heat \end{aligned} \tag{3.3}$$

3.2.2 Photomultiplier Tubes

A photomultiplier tube (PMT) is a device to convert single photons into an electric signal. The principle of a PMT is based on the photoelectric effect combined with the multiplication of charge by using a dynode structure. If the energy of a photon is greater than the work function of a material, the photon can break the bond between an electron and the nucleus and create a free electron. The cross section of the photoelectric effect σ_{Ph} is dependent on the energy of the photon E_γ and the charge number of the absorbing material Z:

$$\sigma_{Ph} \propto \frac{Z^5}{E_\gamma^{7/2}}. \tag{3.4}$$

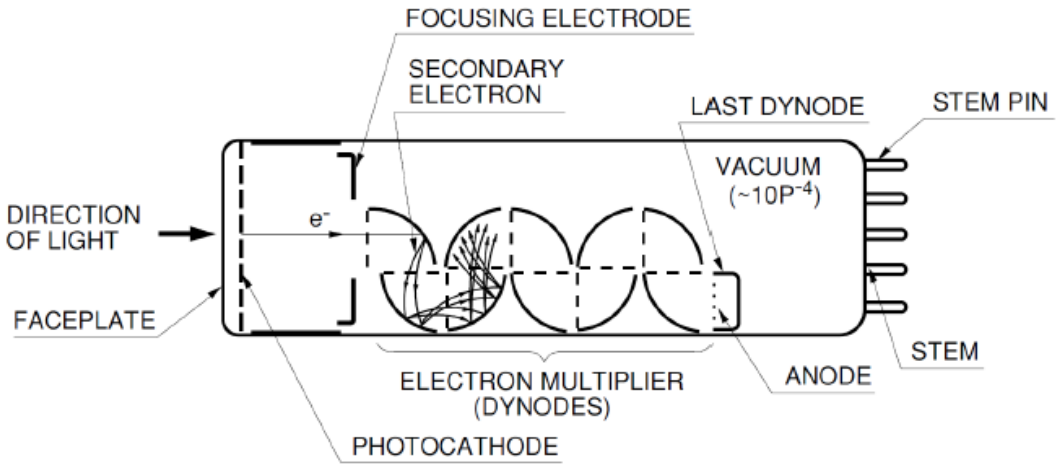

Figure 11: Sketch of a PMT showing the basic principle of multiplying charge with a dynode structure[Ham2006].

Especially for low energy photons like the scintillation light from gaseous xenon, the photoelectric effect dominates the interaction with matter. Thus, PMTs are ideal for detecting low energy photons such as the scintillation light from xenon. Since the photoelectric effect is quantum in nature, it follows a probabilistic distribution. The quantum efficiency (QE) of a PMT quantitatively describes the probability of an incident photon liberating a photoelectron and is defined as:

$$QE(\nu) = \frac{N_{pe}}{N_{ph}}. \tag{3.5}$$

Electrons emitted in the photocathode are accelerated onto the first dynode by a high electric field and a focusing electrode. As seen in figure 11 the electric field is separated by several dynodes with a cascading potential. In every dynode an electron can release several secondary electrons, depending on the applied electric field i.e. the kinetic energy of the electron. By this snowball principle even low energy photons can generate a measurable current at the anode, allowing to count individual photons.

For the krypton monitor a R8520-06-Al Hamamatsu® PMT was used. These PMTs are optimized for the scintillation light of xenon with $\lambda = 178\,\text{nm}$, have an operation temperature range of -110 °C to +50 °C and show extremely low radioactivity. For these reasons they are also used in the TPC in Münster as well as in XENON100. The PMT with an effective area of $(20.5\,\text{x}\,20.5)\,\text{mm}^2$ has a quantum efficiency of $QE(178\,\text{nm}) \approx 30\,\%$. It was implemented in a T-piece with an inner diameter of 36 mm. The inner surface was partially covered with a PTFE foil to increase the light yield. Polished PTFE shows an excellent reflectivity of 99% for photons with wavelengths between 350 nm to 1200 nm. The reflectivity for VUV is yet not sufficiently

understood but definitely increases the light yield as it is estimated for liquid xenon at about (50-90) %[Sil2009]. Furthermore, the reflectivity of PTFE for VUV photons is investigated by the Münster XENON group.

3.2.3 Data Acquisition

At first the signal output from the PMT had to be digitized in order to process it further on. For that, the flash-analog-to-digital-converter (FADC) SIS3320 from Struck Innovative Systeme® was used with a sampling rate of 100 MHz. The SIS3320 is an eight channel FADC with a 12-bit resolution and a voltage range of 0 V - 5 V. The output of the FADC is given in ADC-entities which can be easily converted in voltage counts with the knowledge of voltage range and resolution.

$$1\,\mathrm{ADCE} \hat{=} \frac{5\,\mathrm{V}}{2^{12}} = 1.22\,\mathrm{mV} \tag{3.6}$$

The final acquisition was done by a software package developed at KVI Groningen, controlled by the Java-based program FPPGUI written by Volker Hannen. With that, parameters like threshold or offset of the PMT could be set individually.

3.3 Gas system, TPC and Krypton Distillation Column

For operating a detector like the TPC or the krypton monitor, xenon must be cleaned from any electronegative impurities as they decrease the mean free path of photons drastically and absorb the scintillation light. To remove electronegative impurities a SAES PS4-MT50 heated getter from MonoTorr® was used. It uses a zirconium alloy at a temperature of 400 °C, which forms irreversible chemical bonds with with those impurities, allowing a purification to the sub-ppb level.

The amount water was monitored with a moisture analyzer (Halo+) from Tiger Optics®, which can detect traces of water down to a level of 400 ppt with a sensitivity of 200 ppt. The Halo+ analyzes the signal decay of a diode laser in the sample gas with which a cavity ring is filled. Water would increase the signal decay in the infrared region. The Halo+ is tuned to the signal decay resulting from water and can by that quantify its amount.

The TPC can also allow to monitor the purity of the used xenon by measuring the drift length of electrons in the liquid xenon. However, the TPC was not yet fully operational when the measurements for this thesis were made. It is basically a small version of the TPC used for XENON100. It contains 3 kg liquid xenon with a possible drift length of 17 cm. There are 7 Hamamatsu R8520 PMTs on each top and bottom.

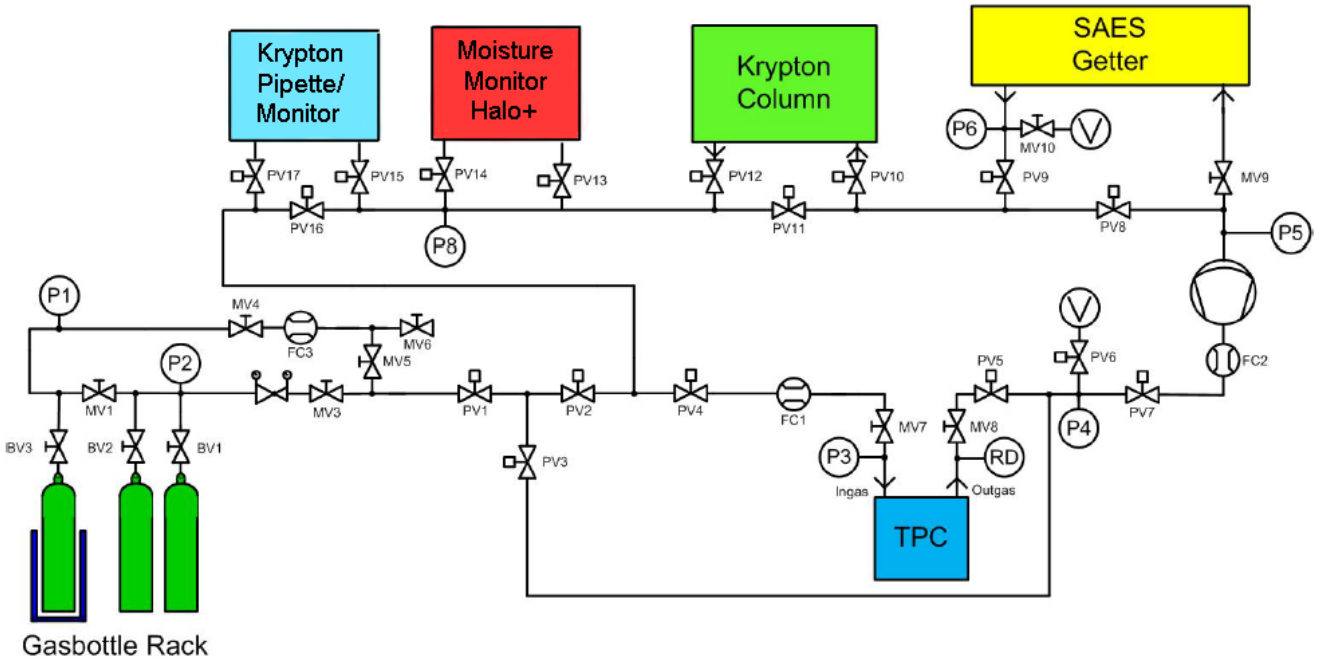

Figure 12: Sketch of the gas sytem build in the laboratory in Münster including the planned krypton distillation column, the TPC, the SAES getter, the moisture analyzer (Halo+) and the krypton pipette.

All elements could be bypassed in order to disconnect them without effecting the rest of the system. To allow a circulation of the gas in the system a diaphragm pump N 0150 ANE from KNF® was used. Multiple digital mass flow controller type 1579 from mks® allowed the control of the gas flow in different segments of the system. Since the gas system was designed to allow high flow rates up to 200 slpm (standard liters per minute), the flow meters from mks® were chosen although having the disadvantage of not providing a high accuracy for small flow rates (± 1 slpm). The system could be additionally monitored by multiple pressure meters, type 121A from mks®. The xenon gas could be recuperated simply by cooling the supplying gas bottle with liquid nitrogen to cryo-pump the xenon into the storage bottle.

4 Analysis of the ^{83m}Kr Measurement

4.1 Prediction of ^{83m}Kr Collection

For calibration applications it is beneficial to have a preferably high signal rate. ^{83m}Kr is obtained as the product of a decay and is therefore dependent on the activity of the rubidium source. Since ^{83m}Kr furthermore decays, its activity can be calculated as a decay chain through:

$$A_{Kr}(t) = A_{Rb}(t_0)\frac{\lambda_{Kr}}{\lambda_{Kr} - \lambda_{Rb}}\left(e^{-\lambda_{Rb}t} - e^{-\lambda_{Kr}t}\right). \tag{4.1}$$

With a decay constant $\lambda_{Kr} = 1.035 \cdot 10^{-4}\mathrm{s}^{-1} >> \lambda_{Rb} = 9.3 \cdot 10^{-8}\mathrm{s}^{-1}$ one would expect the activity of krypton to converge to that of rubidium after a short time, reaching the secular equilibrium. However, since the decay of ^{83}Rb only results in the radioactive ^{83m}Kr with a probability of 74.8 % and the emanation rate of the source is about $\epsilon = (70 \pm 5)$ %, the amount of collected krypton is expected to be smaller. In figure 13 the theoretical predicted activity of the collected ^{83m}Kr from a rubidium source with an activity of $A(t_0)_{Rb} = (164.31 \pm 0.66)$ kBq is shown. It shows that after about $t = 6$ h of collecting, the activity of ^{83m}Kr does not increase significantly anymore. For a calibration, where from a low radioactive ^{83}Rb source as much ^{83m}Kr as possible is requested, it should therefore be collected for at least 6 hours.

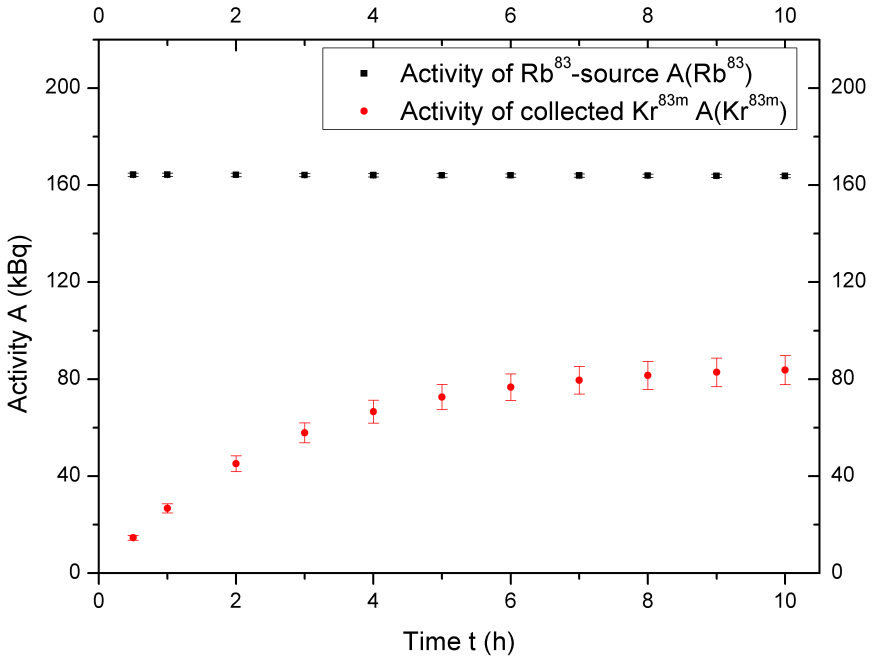

Figure 13: Activity of the radioactive rubidium source and the activity of the collected ^{83m}Kr, considering the decay probability of $P = 74.8$ % and the emanation rate of $\epsilon = (70 \pm 5)$ %.

In practice, one always has to account for the time between the end of collection and the injection of krypton into the gas system. In the case of using the pipette for an energy calibration at XENON100 this time is particular given by the time required for the transportation of the pipette to the underground laboratory. During this time the activity of the collected ^{83m}Kr will decrease exponentially according to equation (2.7).

4.2 Volume of the Gas System

For testing of the krypton pipette, the xenon gas was circulated in a small gas circuit. This small circuit included only the SAES getter, the Halo+ and the KNF pump. To make quantitative statements about the efficiency of the krypton monitor, one first had to know the volume of the gas system in which the collected krypton would be distributed in. The first obvious solution was to simply measure out the length of all pipes while knowing their inner diameter of 10 mm. However, there was no information about the internal gas volume of the bigger parts like the SAES getter, the Halo+ or the KNF pump.

To calculate the unknown volumes a simple pressure analysis was done. The system was first evacuated and then a part consisting solely of pipes and a pressure meter (as seen in figure 12 in between PV3, PV5, PV6 and PV7) with a known volume V_1 and pressure p_1 was filled with a certain amount of xenon gas. To prevent damaging the pressure meter, the pressure had to be hold below the 4 bar level. The rest of the system was segmentally filled with that volume of gas while monitoring the pressure p_2. The temperature could be assumed to be constant, because enough time was provided for the gas to heat up again to room temperature after the expansion in an evacuated segment. Under the assumption of a constant temperature, the additional volume V_2 can be calculated from the pressure ratio.

$$V_1 \frac{p_1}{p_2} = V_{tot} = V_1 + V_2 \tag{4.2}$$

The only exception was the SAES getter. Evacuating the getter was not possible without the risk of damaging it. Instead, it was filled with a known amount of gas with a pressure of 2.31 bar. The procedure of calculating the getter volume was yet the same (except vice versa), since afterwards the gas expanded again in a segment with a known volume V_2, only consisting of pipes and a pressure meter.

With this method the volumes of the relevant parts in the small circuit were determined as below-mentioned in table 1.

Table 1: Calculated volumes by analysing pressure drop while opening the gas system segmentally.

	Pipes+Valves	Pump	Getter	Halo+	Total
Volume [cm^3]	1028±12	30±5	1430±127	50.±10	2540±150

When measurements with the krypton pipette were done, the gas was additionally circulated through the pipette. Its volume could be easily determined, since all parts had known dimensions. The additional volume of the pipette including the krypton monitor was $V_{pip} = (390.9 \pm 11.4)\,\mathrm{cm}^3$, increasing the total volume of the small gas circuit to $V_{tot} = (2930 \pm 160)\,\mathrm{cm}^3$.

4.3 Procedure of a ^{83m}Kr Measurement

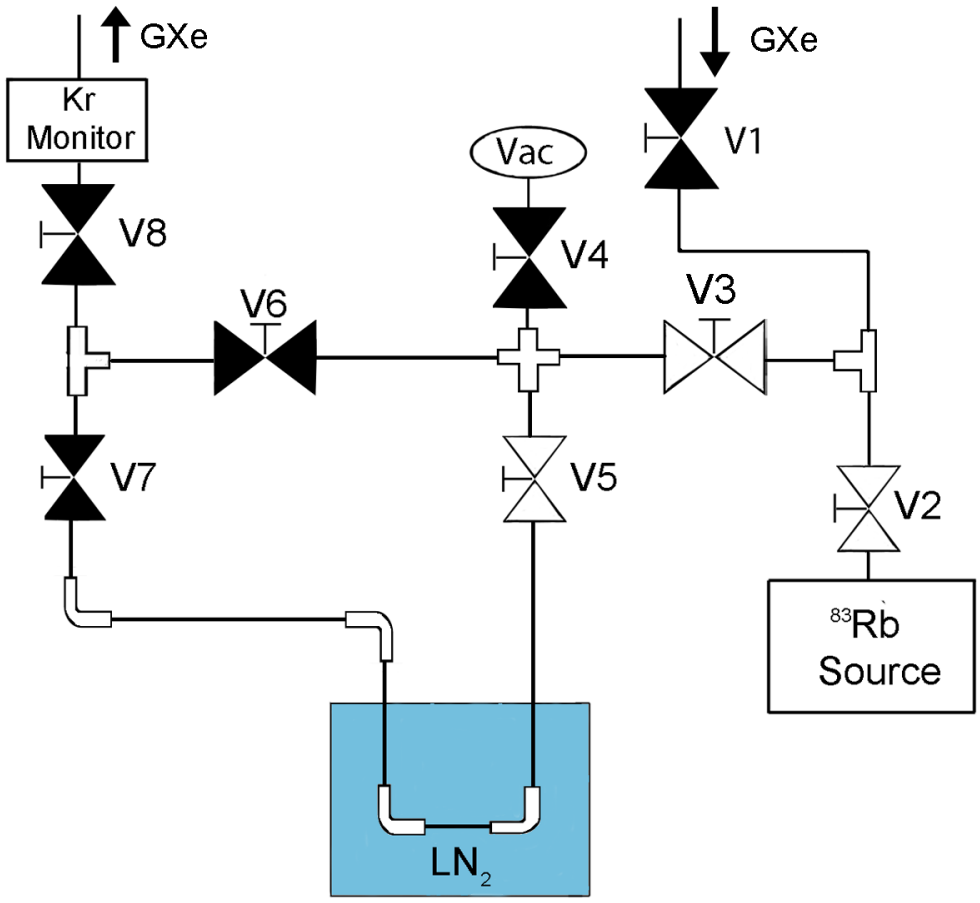

Figure 14: Sketch of the krypton pipette in collecting-mode. White valves indicate to be open while black valves indicate to be closed. In the sketch the cold trap is included, which could be optionally added.

For collecting a specific amount of ^{83m}Kr certain steps had to be made. To assure that the krypton would distribute evenly in the collecting system, it was first evacuated. Therefore all valves except V1, V2 and V8 were opened. After a sufficient vacuum was produced, valves V4, V6 and V7 were closed whereas V2 was opened to start the collecting process. The cold trap with liquid nitrogen (LN_2) could be added optionally. LN_2 cools the collecting segment down to a temperature of $T_{LN2} = 77\,\mathrm{K}$. At 1 atm krypton has a triple point of 116 K and would therefore freeze out at temperatures of LN_2. However, since the amount of collected krypton is about 10^{-15} mol, only partial condensation at the surface of the pipes is expected. This should lead to a higher concentration of krypton in the segment surrounded by the cold trap.

Since for XENON100 the rubidium source had to stay outside of LNGS, the pipette would had to be disconnected at V3 and V8 after collecting. The contaminated parts would have to be evacuated again, before opening to the rest of the system. Therefore only the volume in between V5 and V7 would actually contribute as collecting volume. To allow a comparability, we also decided to use just this volume as collecting volume. Therefore all valves were closed except V3 and V4 to evacuate the remaining volume. If the cold trap was included, it had to be removed and the cooled parts had to be heated up to about room temperature again before opening the pipette to the gas system to avoid condensation of the gaseous xenon. Before the radioactive krypton gas was introduced into the gas circuit, background measurements were done. This allowed a comparison in all measurements of solely the krypton decay after background subtraction.

Finally, to measure the collected amount of ^{83m}Kr V4 was closed whereas V1, V5, V7 and V8 were opened to include the pipette to the remaining gas system. The circulating gaseous xenon would by that be doped with ^{83m}Kr which directly afterwards could be analyzed with the krypton monitor. When calculating the expected activity of ^{83m}Kr inside the krypton monitor, the time between closing the rubidium source and measuring an even distribution of krypton was always accounted for through equation (2.7). The comparison between the expected and measured rate eventually allowed drawing conclusions about the response of the krypton monitor. For all measurements the amount of water as electronegative impurity was measured to be smaller than 3 ppb.

4.4 Collection of ^{83m}Kr with a Krypton Pipette

4.4.1 Collecting without a Cold Trap

When collecting without a cold trap, the emanated ^{83m}Kr is expected to distribute evenly in the opened system with a volume of $V_{distr} = (170.3 \pm 1.1)\,\mathrm{cm}^3$. The actual collecting volume is $V_{coll} = (72.2 \pm 0.4)\,\mathrm{cm}^3$. Therefore, from the total amount of emanated ^{83m}Kr only $G_C = (42.4 \pm 0.4)\,\%$ gets collected. The geometric collecting factor G_C is simply the ratio of both volumes V_{coll}/V_{distr}.

For the first measurement ^{83m}Kr was collected for 6 hours without a cold trap. Gaseous xenon was circulated with a flow rate of $F = (8.3 \pm 1)\,\mathrm{slpm}$ (standard liters per minute) with a gas pressure of $p = (1.07 \pm 0.01)\,\mathrm{bar}$. Without ^{83m}Kr inside of the krypton monitor, a background rate of $r_b = (3.0 \pm 0.2)\,\mathrm{Hz}$ was observed. This rate is mostly determined by electronic noise and ambient radiation, for instant from cosmic rays. The event rate for this measurement is shown in figure 15 and 16.

After opening the pipette at $t = 60\,\mathrm{s}$ the event rate shows a periodic fluctuation with a circulation time $\Delta t = (34.6 \pm 0.4)\,\mathrm{s}$. Here one sees how the krypton circulates with the xenon gas through the gas circuit and after a short time mixes with it due to diffusion and the circulation process. The immediate response and the qualitative behaviour of the fluctuations allows a disregard of complex fluid dynamic effects inside the krypton monitor. ^{83m}Kr shows no clumping or any other behaviour which would require a consideration of it as separate gas.

Furthermore, after ten minutes the fluctuating behaviour dies down and the event rate levels off at about 160 Hz. From that point on the rate decays exponentially, as seen in figure 16. By fitting the curve with an exponential fit, the half-life can be measured and is found to be $t_{1/2} = (1.86 \pm 0.01)\,\mathrm{h}$ which agrees with the literature value of the half life of ^{83m}Kr. This validates that the monitor is actually detecting the decaying krypton. The standard ROOT fitting routine was used with the method of least squares minimization.

The circulation time Δt allows a cross check of the calculated volume of the gas circuit in chapter 4.2. A mass flow meter states the volumetric flow per time at standard conditions ($p_{stp} = 1\,\mathrm{atm}$, $T_{stp} = 0\,^\circ\mathrm{C}$). If one wants to convert the flow rate in an actual volume with laboratory conditions the universal gas law for ideal gases is used:

$$nR = \frac{pV}{T} = \frac{p_{std}V_{std}}{T_{std}}. \tag{4.3}$$

The standard volume is given by $V_{stp} = F \cdot \Delta t$.

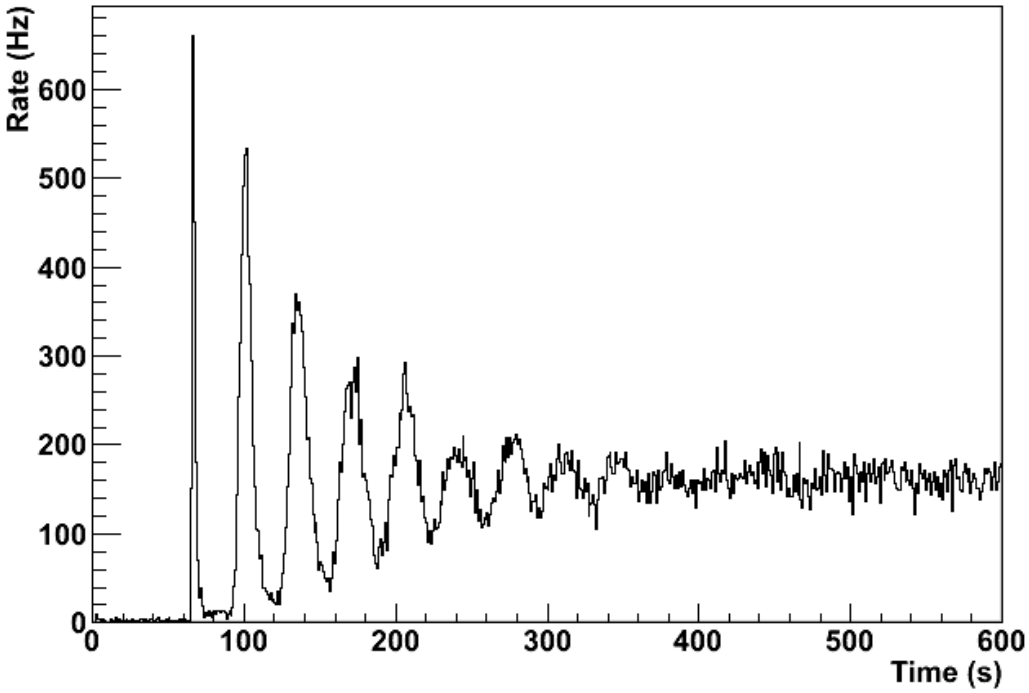

Figure 15: Measured event rate while opening the krypton pipette at $t \approx 60\,\mathrm{s}$ with a flow rate of 8.3 slpm.

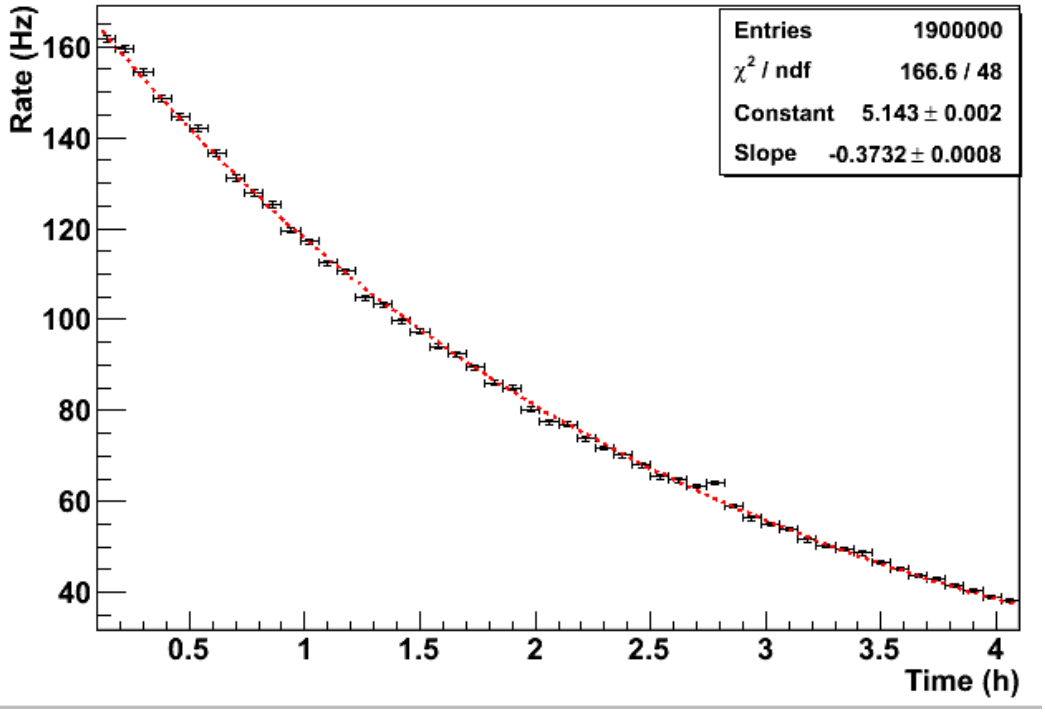

Figure 16: Measured event rate for 4 hours after distribution of krypton at $t \approx 10\,\mathrm{m}$ with a flow rate of 8.3 slpm. The curve was fitted exponentially (dashed red line).

With the actual pressure p and temperature T one can calculate the gas volume with the mass flow F and the circulation time Δt by:

$$V = F\Delta t \frac{p_{stp}}{p} \frac{T}{T_{stp}}. \tag{4.4}$$

Therefore, at a pressure of $p = (1.07 \pm 0.01)\,\text{bar}$ and a temperature of $T = (22 \pm 2)\,^{\circ}\text{C}$ the circulation time $\Delta t = (34.6 \pm 0.4)\,\text{s}$ with a flow rate of $F = (8.3 \pm 1)\,\text{cm}^3$ corresponds to a total volume of $V = (4900 \pm 750)\,\text{cm}^3$. This value disagrees with the calculated volume in chapter 4.2. It is also significantly to high when one regards that the pipe volume can be determined relatively accurate and the pump and Halo+ volume is expected to be roughly as small as determined. This would indicate that the missing volume of about 2 L would be mainly composed by the getter. However, its dimensions make a volume that big not even possible.

This discrepancy could be explained by a higher pessure at the flow controller then the pressure meter indicates or simply suggests that the flow rate at low gas flows may be even less accurate than the specified ±1% of full scale. The volume calculated in chapter 4.2 is more reliable so that for the following calculations a volume of $V_{tot} = (2930 \pm 160)\,\text{cm}^3$ was assumed. Furthermore, for simplification of the calculations an even distribution of the krypton gas is assumed at some point. This is of course just an approximation since the pressure gradiant is not constant within the gas system.

The activity per cm^3 of ^{83m}Kr at the point of even distribution ($t = 10\,\text{min}$) can be calculated to $A_{tot} = (9.8 \pm 0.9)\,\text{Bq/cm}^3$ (in a total volume of $V_{tot} = 2930\,\text{cm}^3$). The volume in front of the PMT in the krypton monitor is $V_{mon} = (132.3 \pm 8.9)\,\text{cm}^3$. Under the premise of having an ideal detector we would expect an event rate of $r_{ideal} = (1296 \pm 148)\,\text{Hz}$. The measured event rate after background subtraction was $r_{meas} = (157 \pm 2)\,\text{Hz}$ with a signal-to-background ratio of $S/B = 52.3 \pm 3.6$.

The signal-to-background ratio is crucial for the use of ^{83m}Kr as tracer for the distillation column. To distinguish a signal from the background one needs at least a signal rate as high as the background rate. Therefore, to make statements about the separation factor of the column the signal-to-background ratio has to be as high as possible.

By comparing the ideal rate to the experimentally measured rate the effectiv volume of the krypton detector can be derived to be $V_{eff} = (16.0 \pm 1.5)\,\text{cm}^3$. With this effective volume the increase of using a cold trap can be evaluated.

4.4.2 Collecting with a Cold Trap

The same measurement as in chapter 4.4.1 was performed with a cold trap, as seen in figure 8 and 14.

The gaseous xenon was circulated with a flow rate of $F = (8.3 \pm 1)\,\text{slpm}$ and a pressure of $p = (0.87 \pm 0.01)\,\text{bar}$. Background measurements showed a rate of $r_b = (2.52 \pm 0.01)\,\text{Hz}$. The event rate, as seen in figure 17 and 18, shows qualitatively the same behaviour as observed before. By fitting the curve in figure 18 exponentially the half-life is calculated to be $\lambda_{1/2} = (1.90 \pm 0.01)\,\text{h}$ which is consistent to chapter 4.4.1. With the assumption that the cold trap would not have an influence in the collection of ^{83m}Kr, the activity per cm^3 at the time of distribution would be $A = (9.0 \pm 0.8)\text{Bq/cm}^3$. With the effective volume of the PMT we would expect to measure an activity of $r_{exp} = (144.0 \pm 12.9)\,\text{Hz}$. A different response of the detector due to the slightly lower pressure was neglected for this purpose (further validation in section 4.5). Temperature- and purity-wise both measurements were taken under similar conditions.

By comparing the expected activity to the measured event rate after background subtraction $r_{meas} = (285 \pm 2)\,\text{Hz}$, we can evaluate the increase of collection by using a cold trap to be a factor of $\alpha = 1.98 \pm 0.18$, which corresponds to a geometric collecting factor of $G_C = (83.9 \pm 7.7)\,\%$. The collection with a cold trap increases the signal-to-background ratio to $S/B = 113.1 \pm 0.9$ at the time of even distribution.

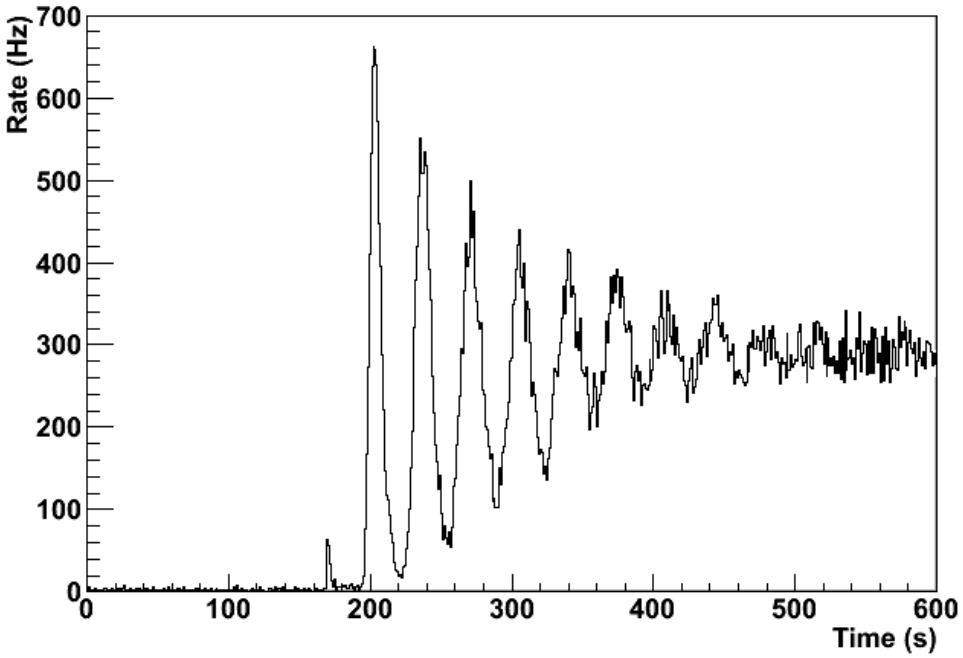

Figure 17: Measured event rate while opening the krypton pipette at $t \approx 180\,\text{s}$ with a flow rate of 8.3 slpm. The collection was done by using a cold trap.

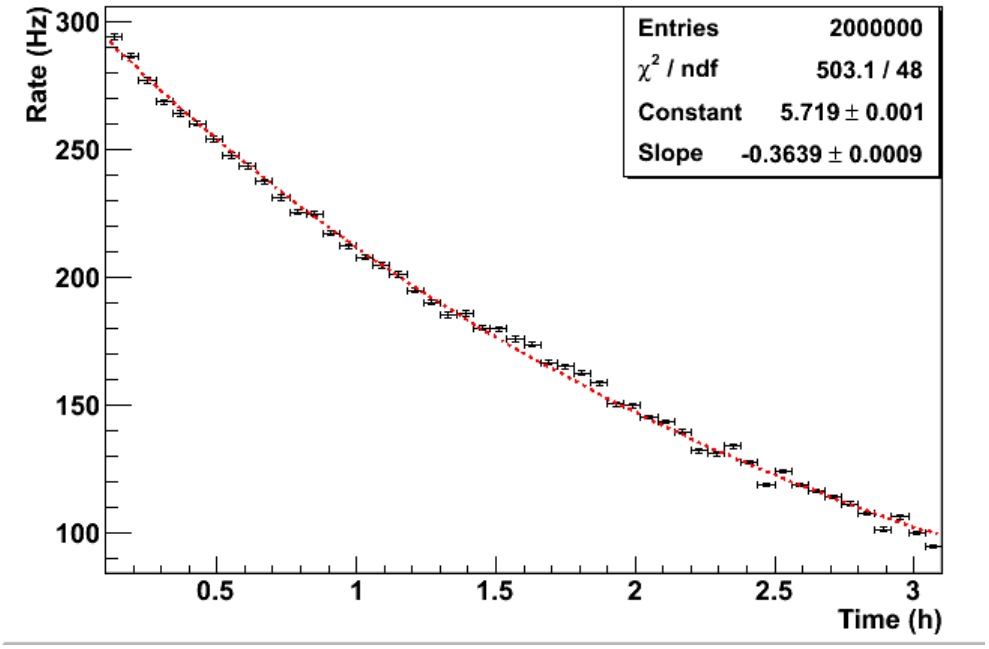

Figure 18: Measured event rate for 3 hours after distribution of krypton at $t \approx 10$ m with a flow rate of 8.3 slpm. The curve was fitted exponentially (dashed red line). The collection was done by using a cold trap.

4.5 Detection of the two Subsequent Decay Steps of ^{83m}Kr by Delayed Coincidence

Another characteristic of the disintegration of ^{83m}Kr than its half-life of 1.83 h is its subsequent decay over the 9.4 keV state with a half-life of 154 ns. This subsequent decay should appear in the waveforms as a two-event signal with a time delay that is consistent with the exponential law from equation (2.5). Since the measured background and the electronic noise should in general not show this characteristic, a decrease of the background rate by analyzing the data for a delayed coincidence is possible and by that potentially an increase of the signal-to-background ratio as well.

In figure 19 an example of a delayed coincidence event is shown with the analysis of the waveform schematically drawn. Events were digitized at 100 MHz with 512 samples per waveform and the trigger at the center of the waveform. Therefore, one expects to see all signals at $t \approx 2600$ ns of the waveform. Small variations are accounted for by searching the first event in a window between 2500 ns to 2700 ns. When a pulse is found that exceeds an amplitude of 12 mV it is accounted as first signal. Then the second event is searched from $t = 2700$ ns on. A pulse exceeding an amplitude of 9 mV then gets accounted as second event. To compare the energy deposit of both signals, an integration is performed over 60 ns after the signal.

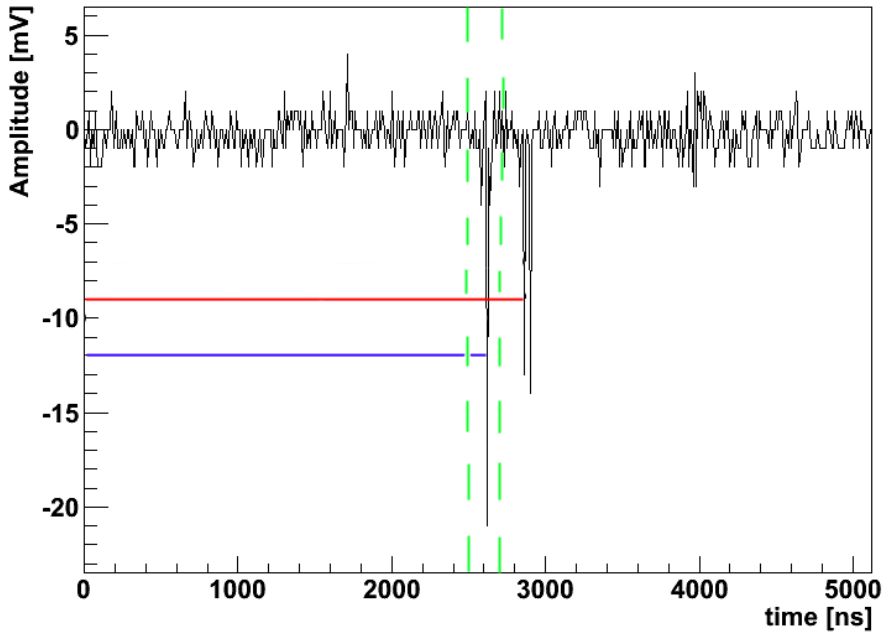

Figure 19: Example of a delayed coincidence event with the schematic of the analysis. The dashed green lines frame the area of an expected signal from the first decay. The second decay is searched for after the second green line. The solid blue/red lines indicates the trigger level for the first/second event.

To avoid fluctuations from the PMT, a baseline subtraction was done for every waveform, where the average voltage of the first 2000 ns gave us the zero line. Since no gain calibration was done for the PMT, the signal could not simply be converted into an energy scale.

Although the FADC with a sampling rate of 100 MHz allowed a resolution of 10 ns, it was not possible to separate two events that sequenced after just few tens of nanoseconds since most events showed a width of about 100 ns. Therefore, the search for the second peak began $t_1 = 130$ ns after the first peak. This obviously excluded many krypton decay events, but showed the best effect on the signal-to-background ratio. In the case of a narrow superposition of first and second decay, the probability rises that a later pulse, which is not correlated to the actual krypton decay will be registered as second event. Therefore only those events that showed a time delay smaller than $t_2 = 800$ ns were accounted as delayed coincident event. The maximal efficiency of this analysis can be calculated to be

$$\epsilon = \frac{\int_{t_1}^{t_2} e^{-\ln(2)t/t_{1/2}}}{\int_0^{\infty} e^{-\ln(2)t/t_{1/2}}} = 52.97\%. \tag{4.5}$$

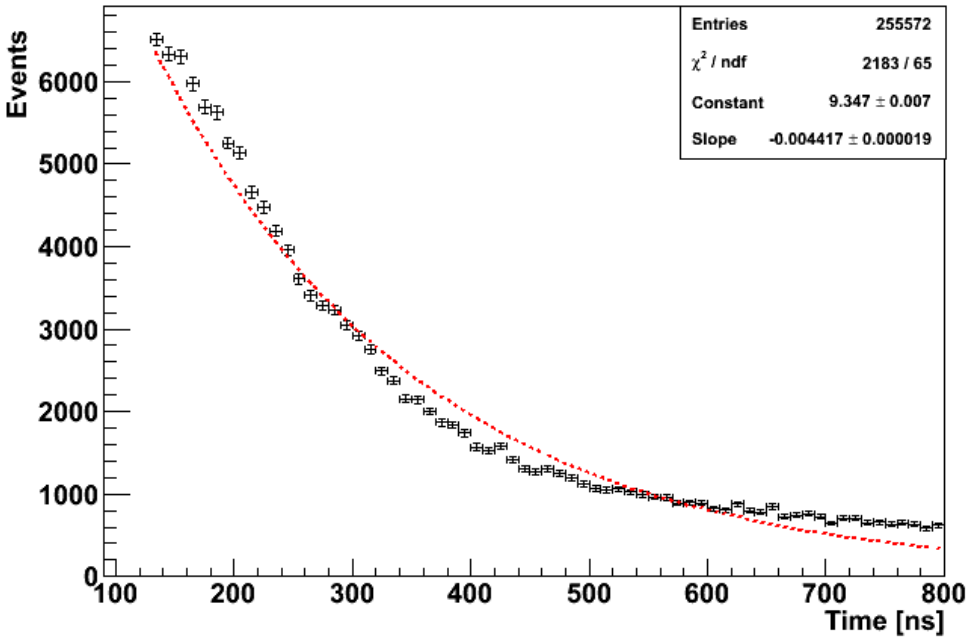

Figure 20: Time delay between first and second event. The curve was fit exponentially (dashed red line).

By analyzing the time delay between two events an exponential behaviour can be observed as seen in figure 20. However, the fit deviates from the actual measurement points (with a reduced χ^2 of about 34). The results show a strong dependency on the area of the fit. The slope of the measurement points deviates especially in the area of high time delays above 600 ns. This was expected due to limitation factors mentioned before. To investigate a statistical error of the delayed coincidence method, four data sets were each analyzed for the time delay between two events and finally fit at different areas of the curve (130 ns-330 ns; 330 ns-530 ns; 530 ns-730 ns). The result is shown in figure 21 where the calculated half-life is plotted against the reduced χ^2. The exponential fits over the whole 800 ns generate a large reduced χ^2 above 45 and are therefore neglected because of their low reliability. Furthermore, the waveforms that induced a delay time over 700 ns were qualitatively analyzed. The majority of them showed a behaviour that could not be explained by the sole decay of a ^{83m}Kr atom. Instead of showing two pulses for the two decays, the waveforms included multiple pulses through the whole 512 samples. A typical waveform that induced a high delay time is shown in figure 22. Here at the trigger a delay coincidence can be observed that was not seperated. Instead additional pulses show up that get mistakenly counted as second decay of ^{83m}Kr. Therefore, the calculated half-life from the exponential fits of the window between 530 ns-730 ns were not considered. With these exclusions the half-life of the secondy decay of ^{83m}Kr is calculated to be $t_{1/2} = (133 \pm 27)$ ns and is within the standard deviation in agreement with the literature value.

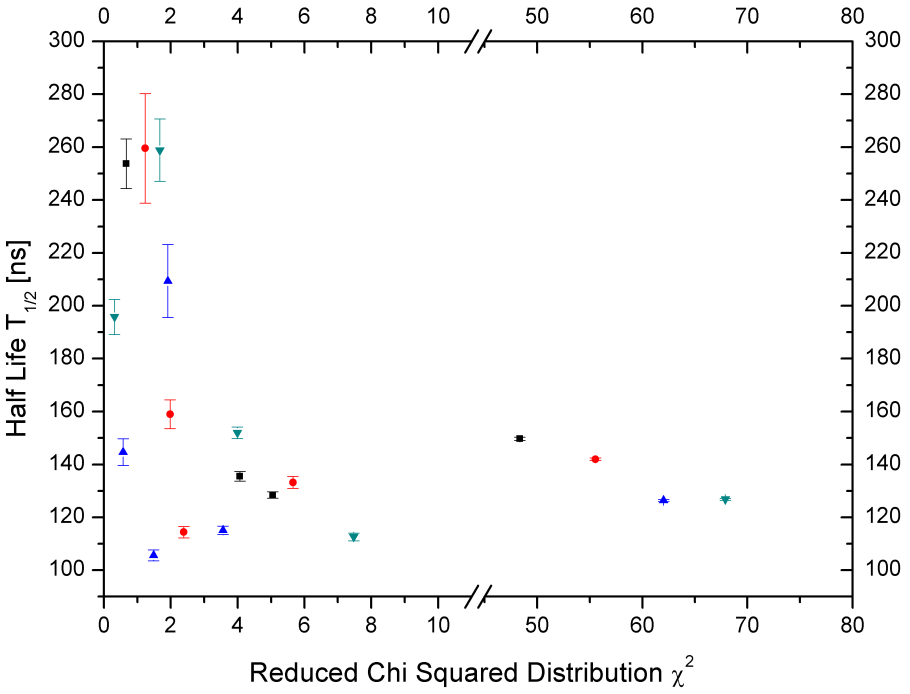

Figure 21: Calculated half-life of the second decay of ^{83m}Kr plotted against the reduced χ^2 from the exponential fit of four different data sets indicated by different colours and shapes. The fits that generated a χ^2 above 45 came from fitting the complete curve, the other ones were due to fitting a certain window of the curve.

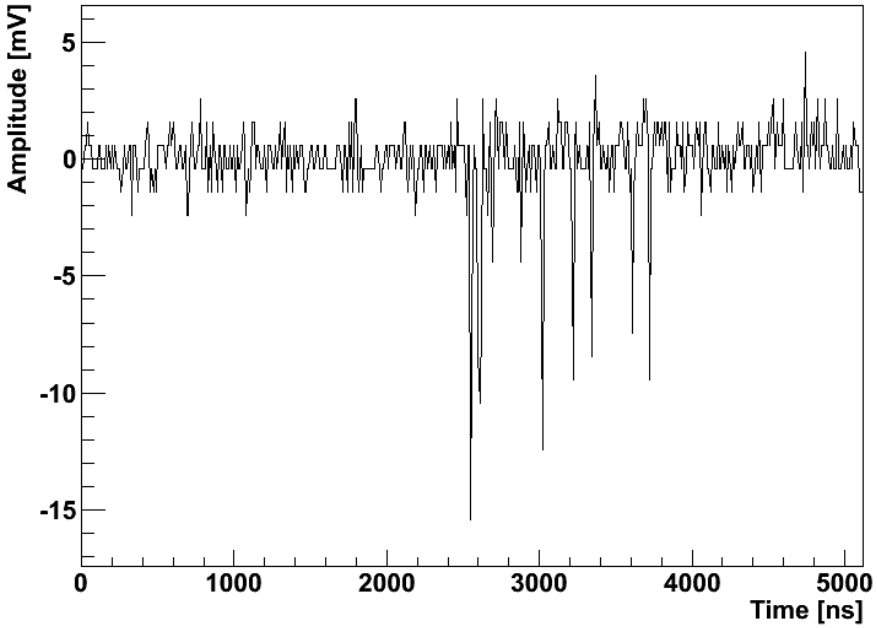

Figure 22: Exemplary waveform of a detected event that suggests a high time delay between a first and a second event.

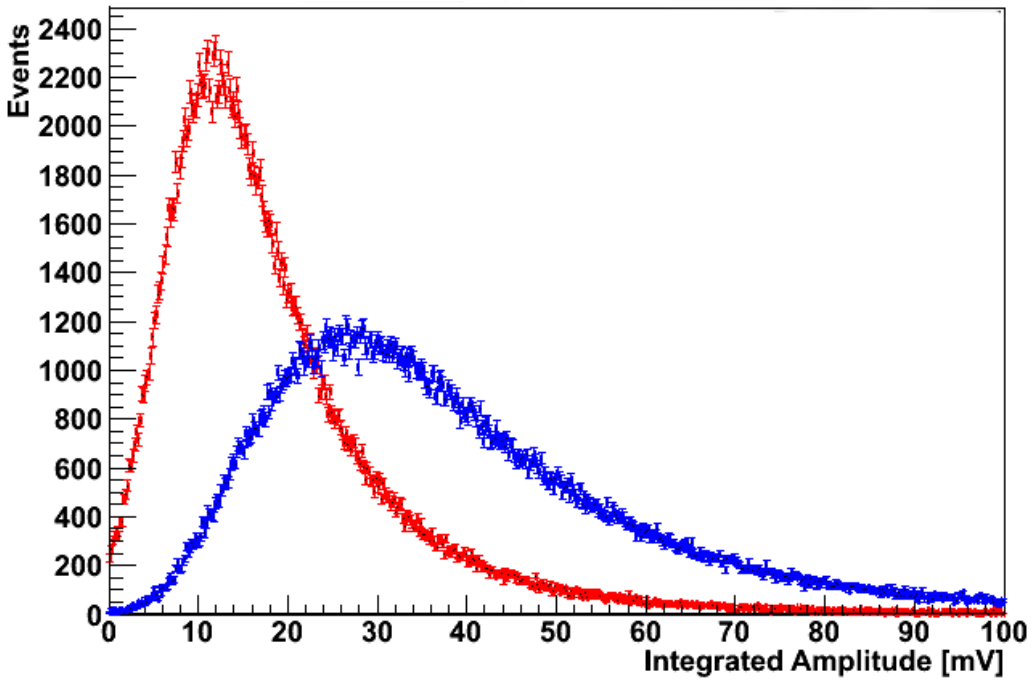

Figure 23: Integrated Amplitude of first (blue) and second (red) event integrated over 60ns. The electronegative impurities in gaseous xenon were measured to be 2.9 ppb.

Furthermore, a light collection analysis can be made for both events. An integration over 60 ns from the signals is shown in figure 23. A separation of both events can be observed in agreement with the different energy levels of the first and second decay from ^{83m}Kr. Both validates that the double coincident analysis of the data taken from the krypton monitor is in fact suitable for finding and processing krypton decay events.

In particular, the light collection analysis of both signals allows one to quantify the response of the PMT to different conditions. The energy of the first decay in figure 23 peeks at about 27 mV. During this measurement the Halo+ measured the amount of water in the xenon gas to be at 2.9 ppb. The value of impurities decreased continuously within the time of our lab work down to 0.6 ppb. The analyzes of the data from this time period shows in correlation to the decreasing impurities a small yet insignificant increase in light yield. At 0.6 ppb the first decay peeks at about 32 mV. Small pressure differences (0.9 bar-1.3 bar) showed no effect in the light yield.

To see what effect the double coincidence method has on the sensitivity of the krypton monitor, the data taken from the measurement in chapter 4.4.2 is processed with the described algorithm. The result is shown in figure 24. The background rate could be decreased by the analysis down to $r_b = (0.17 \pm 0.02)$ Hz while the activity at the time of even distribution shows a

rate of $r_{dc} = (38 \pm 1)\,\mathrm{Hz}$. The signal-to-background ratio increased due to the analysis up to $S/B = 224 \pm 14$, where it was before at $S/B = 113.1 \pm 0.9$.

Under the conditions of this measurement the sensitivity of the krypton monitor can be evaluated, stating the lowest activity per cm^3 A that can still be detected and distinguished from the background.

$$\sigma = A\frac{r_b}{r_{meas}} \tag{4.6}$$

The delayed coincidence method allows a sensitivity of $\sigma_{dc} = (40 \pm 6)\,\mathrm{mBq/cm^3}$. With that sensitivity and under the assumption that significantly higher event rates of about 10 kHz will not affect the sensitivity of the krypton monitor too much, the activity of the ^{83}Rb source can be estimated that would be required to ascertain a separation factor of $S = 10^4$ of the krypton distillation column. In a realistic scenario where it takes about $t_d \approx 20\,\mathrm{min}$ between closing the ^{83}Rb source and having an even distribution of ^{83m}Kr in the gas system, an activity of

$$A_{Rb} = \sigma_{dc} \cdot \frac{V' \cdot S}{\epsilon \cdot P} \cdot e^{\lambda_{Kr} t_d} \approx 4\mathrm{MBq}. \tag{4.7}$$

V' is an estimated volume of 5 L due to the additional volume of the dedicated distillation column.

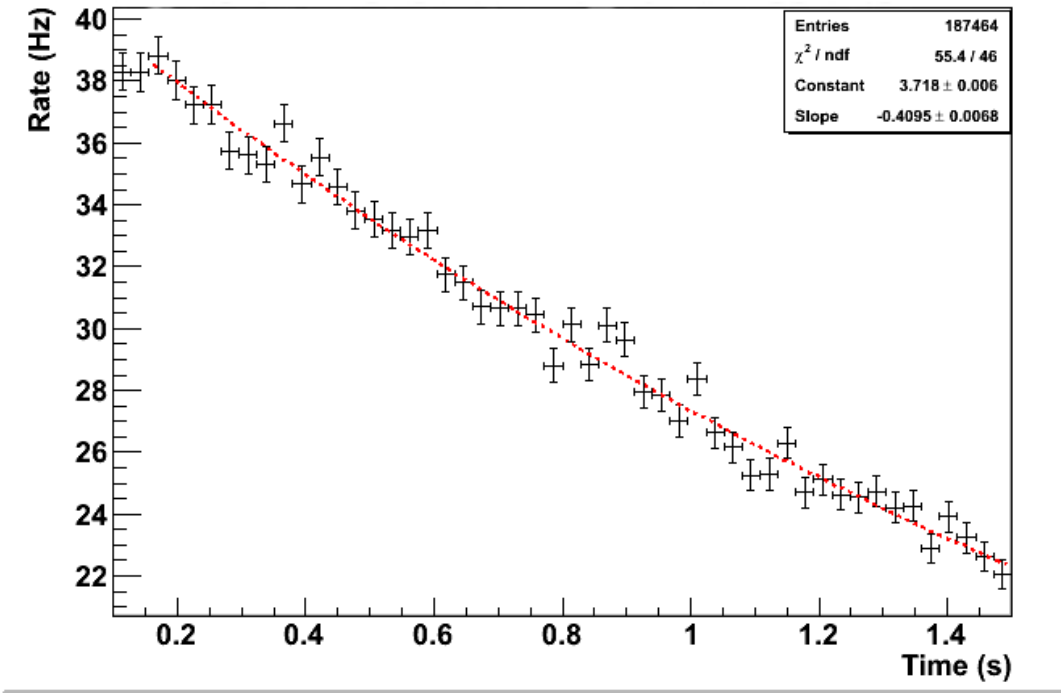

Figure 24: Event rate of the measurement from chapter 4.4.2 with a delayed coincidence analysis. Background measurements showed a background rate of $r_b = (0.17 \pm 0.01)\,\mathrm{Hz}$.

4.6 Effects of Exposing the ^{83}Rb Source to Air

With the knowledge about the response of the krypton monitor, we could investigate what effects exposing the ^{83}Rb source to air can have to the detection rate of our detector. Two possible scenarios could effect the result. First, the electronegative impurities introduced by exposing the system to air could pollute the gas and by that decrease the possible detectable event rate. Secondly, the source itself could be affected by exposing it to air, decreasing the emanation rate for ^{83m}Kr.

For this purpose we disconnected the vacuum pump, opened V2, V3 and V4 and exposed the source to air for 15 minutes. Afterwards, the vacuum pump was reconnected and after closing V2, we evacuated the segment filled with air except the source itself. ^{83m}Kr was collected by using a cold trap. The geometric collecting factor was therefore supposed to be $G_C = (83.9 \pm 7.7)\%$ with an effective volume of the PMT of $V_{eff} = (16.0 \pm 1.5)\,\mathrm{cm}^3$ at a gas pressure of $p = (1.28 \pm 0.01)\,\mathrm{bar}$. Background measurements showed a significantly higher rate at $A_D = (20.6 \pm 0.6)\,\mathrm{Hz}$. After opening the pipette, the expected rate at complete distribution at $t \approx 10\,\mathrm{min}$ would have been $r_{exp} = (166 \pm 26)\,\mathrm{Hz}$. The actual measured event rate after subtraction of the background was $r_{meas} = (140 \pm 2)\,\mathrm{Hz}$, as seen in figure 26, is decreased by 16% but is consistent within the error.

The Halo+ registered no rise in the amount of electronegative impurities (0.9 ppb), although expected. This would imply that a possible decrease in rate originates from decreasing the emanation rate of the zeolite pellets by exposing them to air. However, this is contrary to the results from[Ven2005], where the emanation rate for ^{83m}Kr stays the same for both vacuum (10^{-3} mbar) and air.

By analyzing the collected light from the delayed coincidences a small decrease in light collection can be observed. This would confirm that a possible decrease in rate is in fact induced by pollution of the gas and not by an effect on the emanation rate of the source.

This discrepancy in our measurement can be explained by the position of the krypton monitor and the Halo+ in the gas circuit. The Halo+ was measuring the impurities of the xenon gas, directly after it was purified in the SAES getter. If impurities were introduced by opening the rubidium source, they would effect the krypton monitor, but would not show up as a significant rise of the impurity level in the Halo+.

Furthermore, the analysis of the background showed strong similarities to the decay of ^{83m}Kr, both in terms of the exponential behaviour of delayed coincidences and their energy deposition. The background could not be reduced to a level of about 0.2 Hz, like in every other measurement.

This suggests that the majority of the background is in fact decaying ^{83m}Kr, maybe due to an internal leaking valve. Suppose that the detector would have shown the usual background rate of 3 Hz, the measured rate after background subtraction would have been $r_{meas} = (158 \pm 2)$ Hz and thereby match the expected rate very good, showing an insignificant decrease in rate that could be explained due to the introduced impurities.

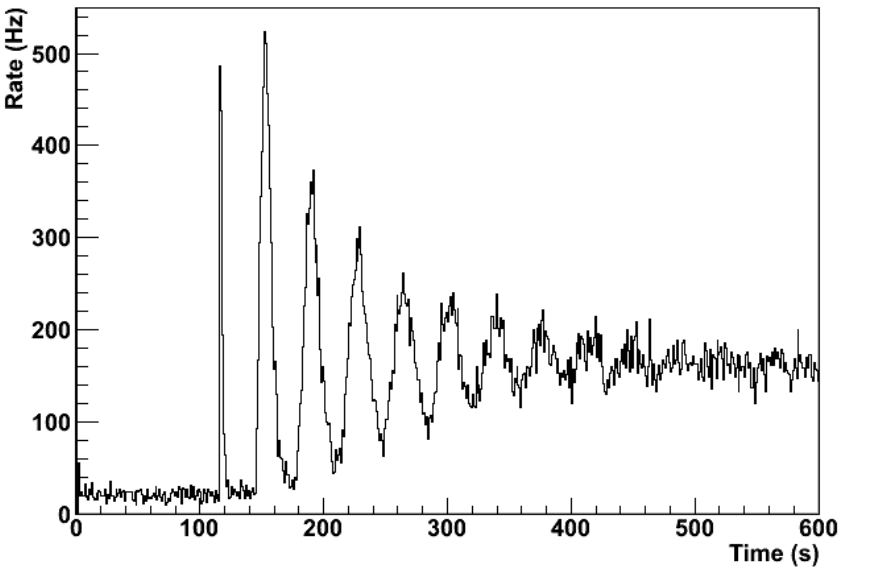

Figure 25: Measured event rate while opening pipette at $t \approx 120$ s with a flow rate of 8.3 slpm. Krypton was collected with a cold trap after exposing the rubidium source to air.

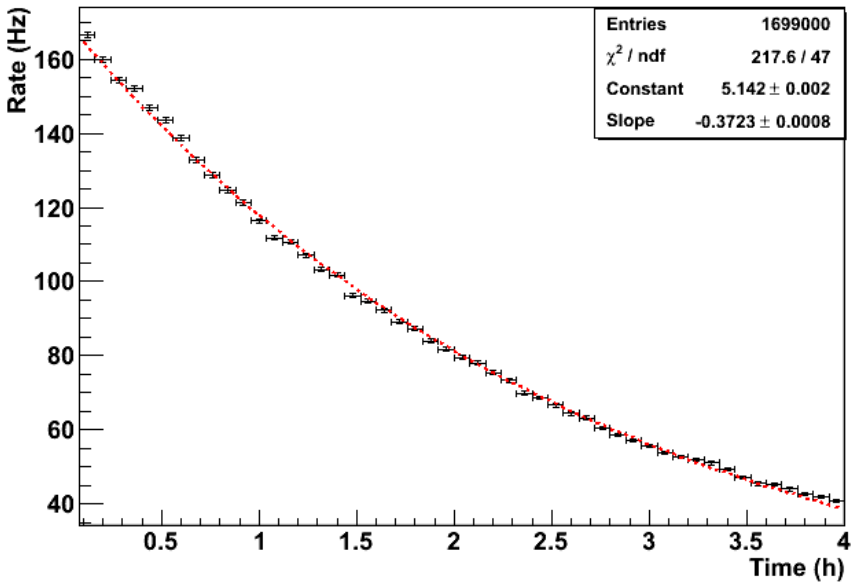

Figure 26: Measured event rate after distribution of ^{83m}Kr. Krypton was collected with a cold trap after exposing the rubidium source to air.

5 Summary and Outlook

Within this bachelor thesis a portable pipette was built which will allow an internal low energy calibration of the XENON100 detector. In this context issues of required purity and maximum collection efficiency were considered. We could show a significant enhancement of the collection by using a liquid nitrogen cold trap. For the collection at XENON100 the cold trap allows practically an almost complete collection of the krypton gas and should therefore be used. The behaviour of krypton doping in gaseous xenon was analyzed and can be stated as suitable for detector calibrations. Since the TPC in Münster was not yet fully operational we could not conform the behaviour of krypton in liquid xenon. This should be an issue of further investigation since it is not yet clear if after liquefication of xenon the krypton will still spread uniformly through it.

To simulate conditions like at XENON100 the rubidium source was exposed to air. We could show that at least a reasonable exposure does not affect the emanation rate of krypton significantly.

Furthermore, in the context of testing if the krypton monitor in Münster is suitable to determine the separation factor of the dedicated krypton distillation column, we could determine the effective detector volume of the PMT to be about $16\,\mathrm{cm}^3$ (for a pressure of 1 bar, an electronegative impurity level of about 2 ppb and the chosen threshold of the PMT at 25 ADCE) and increase the signal-to-background ratio by a factor of two by simply analysing the detected events for delayed coincidences.

To answer the question of the suitability of the krypton monitor for determination of the separation efficiency of the distillation column the conditions under which it will be operated have to be clear. First a smaller column will be tested in Münster to get an understanding of its general properties and behaviour. This test column is not designed to achieve a separation factor of 10^4-10^5 like the one for XENON1T.

If the column will be operated in a dynamic mode with the rest of the system it would be beneficial if for the determination of its separation efficiency the distillation column could be operated in a gas circuit as small as possible since the effective rate is depending on the volume of the gas system. Especially, bypassing the SAES getter for the time of testing would improve the capability of the monitor.

In Münster we can use krypton without the need of collecting it with a portable pipette because the rubidium source is directly connected to the gas system. Any losses from a geometric collecting factor can thus be neglected. Therefore we can expect to collect (in due consideration

of the decay probability $P = 74.8\,\%$ and the emanation rate $\epsilon = (70 \pm 5)\,\%$) a ^{83m}Kr activity of $(52 \pm 4)\,\%$ of the respective ^{83}Rb source activity. At the time when the dedicated distillation column will be operational, the source will have an activity too low to allow convincing measurements. Thus, a new source will be required.

Under these optimal conditions a signal-to-background ratio of ≈2000 would be able to achieve with a ^{83}Rb activity of just ≈1 MBq, allowing a verification of the separation efficiency that is good enough for the small test distillation column.

Still, the delayed coincidence analysis has the potential for optimization. With the chosen window of 130 ns-800 ns and a trigger level of 12/9 mV for the first/second event we achieved an efficiency of just 17 % where the maximal efficiency would be 54 %. Here, especially energy analyses of the waveforms could improve the efficiency for finding delayed coincidences and with that potentially the signal-to-background ratio. Also, increasing the sampling rate to 200 MHz could improve the capability of separating two decays events that follow up in a short time.

In combination with the delayed coincidence method one could investigate if lowering the PMT trigger would improve our signal-to-background ratio. A background measurement with a trigger level of 20 ADCE generated a background rate of (213.1 ± 0.3) Hz. With an analysis of delayed coincidences this rate could be lowered down to (0.101 ± 0.001) Hz which is roughly the same background as for a trigger level of 25 ADCE. If simultaneously more ^{83m}Kr decay events would be registered, a higher signal-to-background ratio can be achieved.

It is very likely that the effective detector sensitivity is affected by significantly higher rates than achieved so far. At very high rates the probability increases that within the sampling time of 5.12 µs multiple events will happen. A possible solution would be to change the number of samples per event down to 256. Since with the delayed coincidence analysis only about 1 µs after the trigger was used, this change would improve our sensitivity for higher rates while still allowing a baseline subtraction over a few hundreds of ns.

Furthermore, the sensitivity of the krypton monitor could be increased by using liquid xenon as scintillation material instead gaseous xenon.

Since the final distillation column is designed to achieve a separation factor of 10^4-10^5, it is very unlikely that its determination can be achieved with the simple method we used so far without the use of a ^{83}Rb source with an unreasonably high activity. At XENON1T a very sensitive mass spectrometer will take over this task.

References

[Abe2009] K. Abe et al.: *Distillation of Liquid Xenon to Remove Krypton.* Astroparticle Physics, V. 31, Issue 4, p. 290-296, 2009

[Apr2004] E. Aprile et al.: *Proportional Light in a Dual-Phase Xenon Chamber.* IEEE Trans. Nucl. Sci. 51, 2004

[Apr2007] E. Aprile et al.: *First Results from the XENON10 Dark Matter Experiment at the Gran Sassor National Laboratory* arxiv:0706.0039v2, 2007

[Apr2009] E. Aprile, T. Doke: *Liquid Xenon Detectors for Particle Physics and Astrophysics.* arxiv:0910.4956v1, 2009

[Apr2012a] E. Aprile et al.: *The XENON100 Dark Matter Experiment.* arxiv:1107.2155v2, 2012

[Apr2012b] E. Aprile et al.: *Dark Matter Results from 225 Live Days of XENON100 Data.* arxiv:1207.5988v1, 2012

[Ari2012] K. Arisaka, D. Cline, C. Ghag: *The XENON1T Dark Matter Project: A Project Proposal from the US Institutions of the XENON Collaboration.* Funding Opportunity Announcement Number: DE-FOA-0000600, 2012

[Ave2012] Avezzano, Sulmona, L'Aquila: *Trasporto singolo occasionale di materiale radioattivo come previsto dal secondo comma dell'articolo 5 della Legge 31 dicembre 1962, N.1860.*

[Beg1991] K. G. Begemann et al.: *Extended rotation curves of spiral galaxies - Dark haloes and modified dynamics.* MNRAS Vol. 249, p. 523-537, 1991.

[Clo2006] D. Clowe et al.: *A direct empirical proof of the existence of dark matter.* Astrophysical Journal 648:L109-L113, 2006

[Ham2006] *Photomultiplier Tubes, Basics and Applications, Hamamatsu Photonics K.K.* 2006

[Han2011] V. Hannen et al.: *Limits on the release of Rb isotopes from a zeolite based 83mKr calibration source for the XENON project.* arXiv:1109.4270v2, 2011.

[Hin2008] G. Hinshaw et al.: *Five-Year Wilkinson Microwave Anisotropy Probe (WMAP) Observations: Data Processing, Sky Maps, and Basic Results.* arXiv:0803.0732v2, 2008.

[Lar2010] D. Larson et al.: *Seven-Year Wilkinson Microwave Anisotropy Probe (WMAP) Observations: Power Spectra and WMAP-Derived Parameters.* Astrophysical Journal Suppl.192:16, 2011

[Man2010] A. Manalaysay et al.: *Spatially uniform calibration of a liquid xenon detector at low energies using 83mKr.* Review of Scientific Instruments 81, 073303, 2010

[Mon2007] C.M.B Monteiro et al.: *Secondary Scintillation Yield in Pure Xenon.* JINST 2 P05001, 2007 [arXiv:physics/0702142]

[Ost2008] Beatrix Ostrick: *Eine kondensierte ^{83m}Kr-Kalibrationsquelle für das KATRIN-Experiment.* PHD-thesis, WWU Münster, 2008

[Pla2012] Guillaume Plante: *The XENON100 Dark Matter Experiment: Design, Construction, Calibration and 2010 Search Results with Improved Measurement of the Scintillation Response of Liquid Xenon to Low-Energy Nuclear Recoils.* Columbia University, 2012

[Oort1932] Jan Oort: *Note on the Difference in Velocity between Absolutely Bright and Faint Stars.* New Haven, Yale University Observatory, 1932

[Sil2009] C. Silva et al.: *Reflectance of the Polytetrafluoroethylene (PTFE) for Xenon Scintillation Light.* arXiv:0910.1056, 2009

[Ven2005] D. Vénos et al.: *^{83m}Kr radioactive source based on ^{83}Rb trapped in cation-exchange paper or in zeolite.* Applied Radiation and Isotopes Vol 62, p. 323-237, 2005.

[Zwi1933] Fritz Zwicky: *Die Rotverschiebung von extragalaktischen Nebeln.* Helvetica Physica Acta Vol. 6, p. 110-127, 1933.

Eigenständigkeitserklärung

Ich versichere, dass ich diese Arbeit selbstständig verfasst habe und keine anderen als die angegebenen Quellen und Hilfsmittel benutzt habe. Zitate wurden also solche kenntlich gemacht.

_____

Münster, 03. August 2012